


EGG-SCM-9576
October 1991

INFORMAL REPORT

EXPERIMENTAL MEASUREMENTS OF PLASMA
PROPERTIES FOR MILLER SG-100 TORCH WITH
MACH I SETTING



**Idaho
National
Engineering
Laboratory**

*Managed
by the U.S.
Department
of Energy*

W. L. T. Chen
J. Heberlein
E. Pfender



*Work performed under
DOE Contract
No. DE-AC07-76ID01570*

Received by OSTI

NOV 22 1991

DISTRIBUTION OF THIS DOCUMENT IS UNLIMITED

This document contains new concepts or the author(s) interpretation of new calculations and/or measurements; accordingly, EG&G Idaho, Inc. is required by the United States Government to include the following disclaimer:

DISCLAIMER

This report was prepared as an account of work sponsored by an agency of the United States Government. Neither the United States Government nor any agency thereof, nor any of their employees, makes any warranty, express or implied, or assumes any legal liability or responsibility for the accuracy, completeness, or usefulness of any information, apparatus, product or process disclosed, or represents that its use would not infringe privately owned rights. References herein to any specific commercial product, process, or service by trade name, trademark, manufacturer, or otherwise, does not necessarily constitute or imply its endorsement, recommendation, or favoring by the United States Government or any agency thereof. The views and opinions of authors expressed herein do not necessarily state or reflect those of the United States Government or any agency thereof.

EGG-SCM--9576

DE92 003309

**EXPERIMENTAL MEASUREMENTS OF PLASMA
PROPERTIES FOR MILLER SG-100
TORCH WITH MACH I SETTING**

**W. L. T. Chen
J. Heberlein
E. Pfender**

**Department of Mechanical Engineering
and
Center for Plasma-Aided Manufacturing
University of Minnesota**

under contract with

**EG&G Idaho, Inc.
Idaho Falls, ID 83415**

Published October 1991

**Prepared for the
Interior Department's Bureau of Mines
and for the
U.S. Department of Energy
Under DOE Contract No. DE-AC07-76ID01570**

OWB
DISTRIBUTION OF THIS DOCUMENT IS UNLIMITED

MASTER

FOREWORD

This work was sponsored by the Interior Department's Bureau of Mines, Contract No. J0134035, under the Department of Energy Contract No. DE-AC07-76ID01570. As INEL's operating contractor, EG&G Idaho, Inc. subcontracted the research reported herein to the University of Minnesota. This contract was initiated under the INEL Strategic and Critical Materials Program, supported and administered by the USBM Materials and Materials Science Division, Dr. Robert J. Kaplan, Chief. George L. Vivian is the Technical Project Officer and Thomas Whittleton is the contract officer for USBM. Victor W. Storhok is Program Manager of the Strategic and Critical Materials Program at EG&G Idaho, Inc. The subcontract was part of the Thermal Plasma Spray Task, Dr. Thomas L. Eddy, Principal Investigator.

CONTENTS

	Page
List of Figures	
List of Tables	
Abstract	1
I. Introduction	2
II. Experimental set-up and procedures	3
III. Experimental results and discussion	7
A. Temperature and velocity fields	7
1. Temperature profiles	7
2. Velocity profiles	9
B. Comparisons of temperature profiles from spectroscopic and enthalpy probe measurements	9
1. Strong discrepancies between temperature profiles derived from two experimental methods	9
2. The dominant effects at different spatial areas in plasma jet and the restriction of spectroscopic measurements	11
3. Error analysis for enthalpy probe measurements	12
C. Plasma composition profiles	13
IV. Summary and conclusions	16
V. References	17
Figures	
Tables	

LIST OF FIGURES

- Fig. 1 Schematic of the integral experimental set-up.
- Fig. 2 Miller SG-100 Mach I plasma gun.
- Fig. 3 Optical system for spectrometric measurements.
- Fig. 4 Schematic of enthalpy probe.
- Fig. 5 Gas sampling line for enthalpy probe measurements.
- Fig. 6 Temperature profiles, plotted as a three-dimensional pattern,
derived from spectroscopic measurements.
Measurement region: $d = 2 \text{ mm} - 30 \text{ mm}$.
($d =$ distance from nozzle exit).
- Fig. 7 Temperature profiles, plotted as a two-dimensional pattern,
derived from spectroscopic measurements.
Measurement region: $d = 2 \text{ mm} - 30 \text{ mm}$.
($d =$ distance from nozzle exit).
- Fig. 8 Isotherms derived from spectroscopic measurements.
Measurement region: $d = 2 \text{ mm} - 30 \text{ mm}$.
($d =$ distance from nozzle exit).
- Fig. 9 Enthalpy profiles, plotted as a two-dimensional pattern.
Measurement region: $d = 30 \text{ mm} - 55 \text{ mm}$.
($d =$ distance from nozzle exit).
- Fig. 10 Enthalpy profiles, plotted as a three-dimensional pattern.
Measurement region: $d = 30 \text{ mm} - 55 \text{ mm}$.
($d =$ distance from nozzle exit).

- Fig. 11 Temperature profiles, plotted as a two-dimensional pattern,
derived from enthalpy probe measurements.
Measurement region: $d = 30 \text{ mm} - 55 \text{ mm}$.
($d =$ distance from nozzle exit).
- Fig. 12 Temperature profiles, plotted as a three-dimensional pattern,
derived from enthalpy probe measurements.
Measurement region: $d = 30 \text{ mm} - 55 \text{ mm}$.
($d =$ distance from nozzle exit).
- Fig. 13 Isotherms derived from enthalpy probe measurements.
Measurement region: $d = 30 \text{ mm} - 55 \text{ mm}$.
($d =$ distance from nozzle exit).
- Fig. 14 Temperature profiles derived from spectroscopic and enthalpy
probe measurements.
Measurement region: $d = 2 \text{ mm} - 55 \text{ mm}$.
($d =$ distance from nozzle exit).
- Fig. 15 Isotherms derived from spectroscopic and enthalpy probe
measurements.
Measurement region: $d = 2 \text{ mm} - 55 \text{ mm}$.
($d =$ distance from nozzle exit).
- Fig. 16 Axial decay of temperature along the centerline of plasma jet.
- Fig. 17 Velocity profiles, plotted as a two-dimensional pattern.
- Fig. 18 Velocity profiles, plotted as a three-dimensional pattern.
- Fig. 19 Velocity isocontours.
- Fig. 20 Axial decay of temperature and of velocity along the centerline
of plasma jet.
- Fig. 21 Mass density profiles.
- Fig. 22 Energy flux profiles.

- Fig. 23 Number densities of particles (unit in cm^{-3}) in argon-helium (100 : 47) thermal plasma of atmospheric pressure at different temperatures.
- Fig. 24 Temperature and plasma composition profiles assuming LTE and derived from spectroscopic measurements ($d = 2\text{mm}$).
- Fig. 25 Temperature and plasma composition profiles assuming LTE and derived from spectroscopic measurements ($d = 10\text{mm}$).
- Fig. 26 Temperature and plasma composition profiles assuming LTE and derived from spectroscopic measurements ($d = 20\text{mm}$).
- Fig. 27 Temperature and plasma composition profiles assuming LTE and derived from spectroscopic measurements ($d = 30\text{mm}$).
- Fig. 28 Temperature and plasma composition profiles assuming LTE and derived from enthalpy probe measurements ($d = 30\text{mm}$).

LIST OF TABLES

- Table 1 Errors in the energy balance of enthalpy probe measurements.
- Table 2 Temperature deviations in plasma jets between spectroscopic
and enthalpy probe measurements.

ABSTRACT

In this work measurements of plasma properties, including the fields of temperature, velocity and plasma composition have been completed for the Miller SG-100 plasma torch using argon-helium mixtures with the Mach I nozzle at 1 atm pressure. A computer-controlled system combining both spectroscopic and enthalpy probe diagnostics has been developed to allow temperature measurements covering a range from 2000 - 16000K which includes the plasma flame region which is of interest. The experimental results expose the dominant effects in different spatial areas of argon-helium plasma jets. In the center near the nozzle exit the temperatures exceed 10000K, and strong diffusion exists due to the steep radial gradients of temperature and particle number densities. In the jet tail region where the temperatures are well below 10000K and decay in axial and radial direction, the dominant effects in this area are strong cold gas entrainment associated with turbulence.

Substantial discrepancies between temperatures evaluated from spectroscopic and enthalpy probe data are particularly severe in the jet fringes indicating that strong deviations from LTE may exist in the jet fringes. In addition, entrainment of the cold surrounding gas into the plasma jet causes severe discrepancies between spectrometric and enthalpy probe data. The validity of the two diagnostic methods will be discussed.

The temperature profiles in argon-helium plasma jets are flatter and wider, and the velocities are higher than in a pure argon plasma jet. These features of argon-helium plasma jets may be beneficial for obtaining better performance in the plasma spraying process.

I. INTRODUCTION

Temperature, velocity and plasma composition are very important plasma parameters for exploiting the optimum operation conditions in high quality plasma spraying. However, it has been found that the physical situation in turbulent plasma jets is rather complicated based on a series of studies in our laboratory ^{1 - 12}. For obtaining precise and reliable results from experiments the diagnostic methods should be carefully selected in dealing with different regimes of plasma jets.

The purpose of this work is to determine the plasma properties in the jet of a commercial torch (Miller SG-100 torch) operated in argon-helium with Mach I nozzle.

A computer-controlled experimental system combining both spectroscopic and enthalpy probe diagnostics has been developed and employed for measuring the temperature and velocity fields in the plasma jets ¹². Spectroscopic methods are used for measuring temperatures above 9000K whereas enthalpy probes are applied for temperature measurements between 2000 and 11000K. In the overlapping regime of the two methods, the temperature profiles from spectroscopic measurements are compared with enthalpy probe data. Substantial deviations, which are particularly severe in the jet fringes, have to be expected. In a series of studies ^{2, 10 - 14} in this laboratory we have found that strong discrepancies between temperatures evaluated from spectroscopic and enthalpy probe data impose severe limitations on the validity of spectrometric temperature measurements in turbulent plasma jets.

The dominant effects, including diffusion effects and cold gas entrainment in argon-helium turbulent jets are considered in connection with the interpretation of experimental results.

II. EXPERIMENTAL SET-UP AND PROCEDURES

A block diagram of the whole experimental set-up is shown in Fig.1. consisting of three parts: a plasma torch system, an enthalpy probe measurement system, and a spectroscopic measurement system.

A commercial d.c. plasma torch (Model Miller SG-100 with Mach I setting: anode 2083-155, cathode 1083A-112 and gas injector 1083A-113), is used as the plasma generator mounted in a water cooled chamber with an opening to the atmospheric environment. A schematic of the plasma torch is shown in Fig.2. The torch current is 800A and the primary gas for the plasma jet is argon with a flow rate of 100 SCFH. The secondary gas is helium with a flow rate of 47 SCFH.

An OMA III (Optical Multichannel Analyzer III), Model 1460-V EG&G PARC, is used to acquire and display spectral data, including the wavelength and intensity of the spectra emitted by the plasma. For imaging the plasma jet onto the entrance slit of the spectrometer an optical system has been designed which is composed of two achromatic lenses and three mirrors as shown in Fig.3. This optical arrangement is suitable for spectral data acquisition in radially symmetric light sources. A 2:1 reduced image of the

plasma jet in side-on observation is cast on the entrance slit of the spectrometer (model HR320, Instruments SA Inc; grating: 1800 lines/mm; entrance slit width: 0.025mm, linear dispersion in first order of the grating: 18 Å/mm). This magnification of the optical system is kept constant during the scanning procedure. The axial position along the plasma jet is controlled by proper positioning of mirror 1 and lens 1 which are driven by two stepping motors which, in turn, are energized by the controller (Model Velmex 86mm-2 interfaced with the OMA 1460-V). The vidicon detector (Model 1254 in the OMA system) is turned by 90° and installed in the exit focal plane of the spectrometer. The detector controller (Model 1216) is interfaced with the OMA-1460V and the vidicon detector. This vidicon detector consists of a two-dimensional photodiode array (silicon intensified target) with 512 x 512 elements which is scanned by an electron beam from left to right and bottom to top, called channels and tracks, respectively, covering a scanning pattern of 12.5mm x 12.5mm. The scanning time along one channel requires 60 microseconds. Horizontal scanning is assigned to the location in the plasma, and the different tracks correspond to the different wavelength of the plasma radiation. The spectrometer and all optical components are arranged on a 60cm x 120cm optical table. The optical system has been precisely aligned with a laser beam. The advantage of this design is its convenience for spectral data acquisition and processing and it will also keep the errors associated with the measurements to a minimum.

The spectral intensity calibrations have been performed by using a Pyrometric MOLARC lamp (Model 2371)¹⁵. Using a set of neutral filters, the useful range can be found as a linear relationship between the counts from the two-dimensional vidicon detector and the spectral intensities from the light source. The transmittance of the Pyrex window of the chamber

has been calibrated. The noise background in the intensity measurements of the argon continuum at a wavelength of 431.2nm and of an argon atomic spectral line at a wavelength of 430.0nm are subtracted from the measured spectrum. For determining spectral line intensities, the continuum background is also subtracted from the total spectral intensities. Radial distributions of the absolute emission coefficients of the argon continuum or of an atomic spectral line from the plasma jet are obtained by Abel inversion 16 - 17. Axial distributions of the absolute emission coefficients are obtained at 2.0mm increments from the nozzle exit of the plasma torch to a distance of 30mm downstream. The applied spectroscopic method based on LTE is valid in the area of the jet axis and near the nozzle exit within the temperature range from 9000 to 16000K.

For extending the temperature profiles and isotherms to lower temperature levels, an enthalpy probe method has been used. An enthalpy probe is generally considered to be a reliable diagnostic tool in the temperature range from 2000 to 10000K 7 - 8. This diagnostic tool allows measurements of composition, temperature and velocity in plasma jets.

The enthalpy probe measurement system (Fig. 1) includes a water-cooled enthalpy probe, a probe cooling system, a gas sampling line, a probe traversing mechanism and a data acquisition and control unit.

The enthalpy probe with an outer diameter of 3.048mm and a sucking port of 0.686mm, consists of stainless steel and has been designed in the High Temperature Laboratory and built by the Physics Department Shop at the University of Minnesota (Fig. 4). The cooling water of the probe cooling system is pressurized by a helium source. Two thermocouples are located at the coolant channel outlet and inlet for measuring the cooling water temperature increase. The third thermocouple is installed at the end of the

sucking port of the probe and connected to an electronic icepoint for measuring the gas sample temperature. Using the enthalpy probe, the values of local enthalpies in the plasma can be measured. Enthalpy values of the jet are obtained from an energy balance applied to the cooling water flowing through the probe and the gas sample continually being extracted from the plasma. For eliminating external heat transfer to the probe a "tare" measurement is required. The temperature increases are measured, respectively, with sample gas flow and without sample gas flow from the plasma through the probe. This "tare" measurements (no flow) are controlled by two electro-valves connected to the data acquisition unit Model HF3421A. The gas sampling line shown in Fig. 5 is used to determine the sample flow rate. A sonic orifice is adjusted to a critical condition for the gas sample flow around 10 mg/s. During the flow period, the pressure P_0 and the temperature T_0 immediately upstream of the sonic orifice are measured with a thermocouple and a piezoelectric pressure transducer, respectively. During the no-flow period, the stagnation pressure P_{st} and the temperature T_s are also measured. The experimental parameters are averaged for 10 measurements. Before starting the data acquisition, the geometric center of the plasma jet is found by using a laser beam and a corresponding optical system. Then the actual center position of the plasma jet is determined by measuring the stagnation pressures while traversing the probe along two horizontal directions. Data acquisition is entirely computer-controlled.

For a conversion of enthalpies into temperatures or stagnation pressures into velocities, knowledge of the thermodynamic state of the plasma which is based on the modeling work in this laboratory 18 - 19 is required.

III. EXPERIMENTAL RESULTS AND DISCUSSION

A. TEMPERATURE AND VELOCITY FIELDS

1. Temperature profiles

Temperature measurements for the Miller SG-100 plasma torch with the Mach I setting have been performed using the spectrometric measurement system. Spectrometric measurements of the absolute emission coefficients of the argon continuum and of atomic spectral lines have been restricted to temperatures above 9000K. This method covers a range from the nozzle exit to less than 30mm downstream and extends to less than 5mm in radial direction.

Plasma temperatures are determined from absolute emission coefficients of the argon continuum at a wavelength of 431.2nm or from an argon atomic line at a wavelength of 430.0nm. The plasma equations based on LTE and optically thin conditions have been applied 20 - 22.

Experimental results based on spectroscopic measurements are shown in Figs. 6 as three-dimensional plots, as two-dimensional plots with the distance d from the torch nozzle exit as parameter (Fig. 7),and as isotherm field (Fig. 8).

The enthalpy probe measurements cover an axial range from 30 mm to 55 mm and a radial range from 0 to 10 mm. The profiles of enthalpy, temperature and isotherms derived from the enthalpy probe measurements

are shown in Fig. 9 - 13. Downstream the jet flame spreads out to a larger diameter and simultaneously the temperatures drop below 5000K. The lower temperatures account for higher densities and lower viscosities in the plasma, so that the local Reynolds number (the ratio of inertia and viscous forces) increases with distance from the nozzle exit. The spreading phenomena of the jet flame reflect the turbulent characteristics of the downstream part of the plasma jet.

Combining the results from spectroscopic and enthalpy probe measurements, the radial temperature profiles and isotherms of the plasma jet are shown in Fig. 14 and 15, respectively. The temperature profiles shown in Fig.14 clearly reflect the entrainment of the cold surrounding gases into the plasma jet. Strong deviations between spectrometric and enthalpy probe data occur in the jet fringes indicating that cold gas already penetrated into this region at distances $d > 30\text{mm}$ from the nozzle exit. In Fig. 15 the isotherms are almost parallel in the region near the nozzle exit where the temperatures exceed 10000K. This behavior reflects the laminar characteristics of the jet near the nozzle exit region. The transition from laminar to turbulent flow occurs around 35mm downstream from the nozzle exit.

The axial decay of temperatures along the centerline of the plasma jet is shown in Fig. 16. The break of the curve at $d=30\text{mm}$ indicates a strong discrepancy between spectrometric and enthalpy probe data in this region which will be discussed in section B.

2. Velocity profiles

The velocity profiles and velocity isocontours derived from stagnation pressure measurements are shown in Fig. 17 - 19. Unfortunately, the velocity measurements shown in these diagrams could not be extended to $d < 30\text{mm}$, because of probe overheating problems. Since the maximum velocity at $d = 30\text{mm}$ already reached 600 m/s , it is conceivable that the velocity close to the nozzle exit may be as high as 800 m/s . Compared with the corresponding profiles in pure argon plasma jets (argon flow rate $m = 100\text{ SCFH}$ and arc current $I = 800\text{ A}$), the velocities in the Ar-He jets are approximately 10% higher and the profiles are approximately 10% wider. This explains why Ar-He mixtures are frequently used for commercial spraying.

The axial decay of the velocity along the centerline of the plasma jet is shown in Fig. 20. For comparison with the temperature decay, the centerline temperatures are also plotted in this figure.

B. COMPARISONS OF TEMPERATURE PROFILES FROM SPECTROSCOPIC AND ENTHALPY PROBE MEASUREMENTS

1. Strong discrepancies between temperature profiles derived from the two experimental methods

Temperature profiles and isotherms derived from spectrometric and enthalpy probe measurements at $I = 800\text{A}$ have been shown in Figs. 14 and 15.

As previously mentioned, the strong discrepancies between temperatures derived from spectrometric and enthalpy probe data are

primarily due to the entrainment of cold gas into the downstream region of the plasma jet. Previous measurements in pure argon ¹² have shown that close to the nozzle exit where the cold entrained gas did not yet reach the core of the plasma jet, spectrometric and probe data are in good agreement, but strong deviations still exist in the fringes.

Since the jet appearance as well as the measured isotherms in the case of Ar-He mixtures indicate that the jet up to around $d=30\text{mm}$ is essentially laminar, the discrepancy of spectrometric and enthalpy probe data cannot be associated with gas entrainment. There are indications that this deviation in the fringes is due to diffusional effects. Because of steep radial gradients close to the nozzle exit, high energy electrons will diffuse towards the jet fringes causing collisions with neutral atoms higher population densities of excited states. These higher population densities lead to an overestimate of spectroscopically determined temperatures, i.e. deviations from LTE ²⁴ occur in this region. In the center of the plasma jet at $d=30\text{mm}$ the percentage of the temperature deviation is close to 20%. This discrepancy is beyond the error limits of both spectrometric and enthalpy probe measurements. Considering the fact that velocities in Ar-He plasma jets are substantially higher than those in pure argon jets, these high axial velocities may give rise to delayed chemical reactions, i.e. the electron population may exceed equilibrium values in the axis. In other words, the plasma in the jet axis may approach chemically "frozen" conditions, a situation which is well known from low pressure plasma jets. Similar as in the previously described case of diffusion of electrons into the jet fringes, the higher electron densities in the axis due to frozen chemistry will lead to higher population densities of excited states and, therefore, to higher temperatures inferred from spectroscopy. Although this explanation appears reasonable, measurements

of electron densities close to the nozzle exit should be made to prove this point. The observed temperature discrepancies become more severe with increasing radius and may reach values as high as 45% at a radius of $R=3\text{mm}$ (see Table 2). These severe deviations have been also observed at different current settings (from 300A to 800A) in pure argon plasma jets with flow rates of 75 SCFH (see Table 2).

2. The dominant effects at different locations in the plasma jet and restrictions on spectroscopic measurements

As previously mentioned, diffusion processes are responsible in the laminar regime of the plasma jet for the observed temperature discrepancies in the jet fringes ²⁴. Thermal diffusion due to temperature gradients and ordinary diffusion due to particle density gradients lead to an overpopulation of charged particles in the jet fringes. The emission coefficient of the argon continuum, for example, is directly proportional to the square of the electron number density. Therefore the spectrometric measurements will indicate higher temperatures in the fringes of the plasma jet.

The temperature discrepancies based on spectrometric and enthalpy probe measurements and observed in different regimes of the plasma jet may be classified as follows:

- a) Temperature discrepancies in the fringes close to the anode nozzle exit ($d < 30 \text{ mm}$ — laminar regime of the jet) are believed to be due to diffusional effects.

- b) Temperature discrepancies in the axis of the jet, but still in the laminar regime are probably due to a transition towards frozen chemistry, caused by the high axial velocities in the jet.
- c) For temperature discrepancies further downstream ($d > 35$ mm) where turbulence governs the behavior of the plasma jet, cold gas entrainment will be the dominant reason.

These findings limit the validity regime for the application of spectroscopy in such jets. For the present conditions, this regime comprises the core of the plasma jet for probably $d < 20$ mm.

3. Error analysis for enthalpy probe measurements

For checking the overall accuracy of the enthalpy probe measurements, energy and mass balances in the plasma jets have been performed.

The errors in the energy balances are expressed as the percentage difference between the integrated energy flux and the net power transferred to the plasma through a certain cross section at a given axial location. A similar procedure is applied to the mass balance. The mass density profiles of the plasma jet are shown in Fig. 21 and the energy flux profiles in Fig. 22. The errors in the energy balance for enthalpy probe measurements are shown in Table 1. As expected, for the entire range of measurements, the errors are negative, i.e. some of the energy in the jet fringes is not measured because of the low sensitivity of the probe in this low temperature region. This error analysis provides a good confirmation of the validity of enthalpy, temperature and velocity measurements with this probe method. In our measurements, the enthalpy probe is also used as a water-cooled pitot tube to

measure the stagnation pressure during the no-flow period. Then the Bernoulli theorem is applied to determine the free-stream velocity. The velocity measurements based on the Bernoulli theorem are valid as long as the Reynolds number based on the probe diameter remains sufficiently high. 7 - 8 According to an error analysis²³ on the effect of temperature gradients in the boundary layer of a pitot tube on the velocity measurements, a water-cooled probe can be safely used for the measurements of the velocity in plasma flows. The maximum error due to temperature gradients is less than 10%, probably around 5% or less over the cross section of the thermal plasma flow.

Therefore, the enthalpy probe method based on the principles of thermodynamics and heat transfer for determining temperature and velocity profiles is a reliable and meaningful diagnostic tool for investigating plasma properties in argon-helium jets, particularly for those plasma plume areas in which strong cold gas entrainment is involved and the spectroscopic methods are no longer valid.

C. PLASMA COMPOSITION PROFILES

The composition profiles for argon-helium thermal plasma at 1 atmospheric pressure have been calculated with the assumption of local thermal equilibrium (LTE).²⁵

The equilibrium equations include two Saha equations for argon and helium, Dalton's law, the initial constant ratio of argon to helium, and the electrical neutrality relation for plasmas :

$$\frac{n_{Ar+}}{n_{Ar}} = \frac{1}{n_e} \frac{2 Z_{Ar+}}{Z_{Ar}} \frac{(2\pi m_e kT)^{3/2}}{h^3} \exp \left\{ - \frac{E_i (Ar) - \Delta E_i(n_e)}{kT} \right\} ,$$

$$\frac{n_{He+}}{n_{He}} = \frac{1}{n_e} \frac{2 Z_{He+}}{Z_{He}} \frac{(2\pi m_e kT)^{3/2}}{h^3} \exp \left\{ - \frac{E_i (He) - \Delta E_i(n_e)}{kT} \right\} ,$$

$$P = (n_e + n_{Ar+} + n_{Ar} + n_{He+} + n_{He}) kT ,$$

$$\frac{n_{Ar+} + n_{Ar}}{n_{He+} + n_{He}} = \frac{100}{47} ,$$

$$n_{Ar+} + n_{He+} = n_e ,$$

where n_e , n_{Ar} , n_{Ar+} , n_{He} and n_{He+} are the number densities of electrons, argon atoms, argon ions, helium atoms and helium ions, respectively. P is the total pressure, k is the Boltzmann constant and T is the temperature. Z_{Ar} and Z_{Ar+} are the partition functions of argon atoms and ions, respectively. Z_{He} and Z_{He+} are the partition functions of helium atoms and ions. E_i is the ionization potential and ΔE_i represents the lowering of the ionization potential. m_e is the electron mass, and h is Planck's constant.

The plasma composition in an Ar-He plasma includes five species, i.e. n_e , n_{Ar} , n_{Ar+} , n_{He} and n_{He+} (unit : particle numbers / cm^3). The

number densities of particles in an argon-helium (initially 100 : 47) thermal plasma at atmospheric pressure at different temperatures are shown in Fig. 23. The temperature and plasma composition profiles assuming LTE and derived from spectroscopic temperatures are shown in Figs. 24 - 27 for different distances from the nozzle exit. The temperature and plasma composition profiles assuming LTE and derived from enthalpy probe temperatures at $d=30\text{mm}$ are shown in Fig. 28. For $d = 2 \text{ mm}$, the steep radial gradients of temperature cause strong diffusional effects. The electron number densities near the jet center are higher than the number densities of argon and helium atoms, since ionization of argon plays an important role for temperatures around 15000K. For this temperature, however, the number densities of helium ions and the degree of ionization of helium gas are still much lower in comparison with those parameters for argon (see Fig. 24) since the ionization potential of helium (24.58 eV) is much higher than that of argon (15.8 eV).

According to the composition calculations ²⁶ for argon-helium plasmas at 1 atm in which the diffusion effects were considered, the argon concentration does not deviate much from the LTE concentration, but the helium concentrations near the center increase about 50% for higher temperatures ($T_0 = 15000\text{K}$). For the lower temperature range ($T_0 = 12000\text{K}$), the composition with diffusion effects included almost follows the LTE composition. These calculations indicate that when we use spectroscopic methods for determining temperatures of argon-helium thermal plasmas at 1 atm, we should select argon spectra rather than helium spectra in order to obtain valid results.

IV. SUMMARY AND CONCLUSIONS

Measurements of plasma properties, including the profiles of temperature, velocity and plasma composition, have been performed for the Miller SG-100 plasma torch with Mach I setting and an arc current of 800 A. An argon-helium mixture has been used with flow rates of 100 and 47 SCFH, respectively.

An integral measurement system, consisting of a spectroscopic facility (OMA system) and an enthalpy probe system, allows measurement of temperatures covering a range from 2000 - 16000K which matches the entire regime of a plasma jet (axial distances within 55 mm and a plasma radius up to 10 mm). Data acquisition and processing are computer-controlled.

The spectroscopic measurements are used to determine the temperature fields in the core of the plasma jet near the nozzle exit where temperatures exceed 10000K. In this regime laminar flow prevails and diffusional effects have to be taken into account. The enthalpy probes are used to determine temperatures up to 10000K, average temperatures in turbulent jet regimes (hot plasma and cold entrained gas), and the velocity fields of the downstream areas where the temperatures fall below 10000K and where spectroscopic methods are no longer valid. The downstream areas of the jets are characterized by turbulent flow and strong cold gas entrainment.

Discrepancies between temperatures evaluated from spectroscopic and enthalpy probe data are particularly severe in the jet fringes indicating that strong deviations from LTE may exist in the jet fringes or that cold gas entrainment biases spectrometric measurements..

In addition, deviations from chemical equilibrium are believed to be responsible for the observed temperature discrepancies in the axis of the jet for $d = 30$ mm. In order to prove whether or not the explanation offered for temperature discrepancies close to the nozzle exit is correct, electron density measurements should be made using Stark broadening.

The temperature profiles in argon-helium jets with Mach I setting are flatter and wider, and the velocities are higher compared with those in pure argon jets. These features are characteristic for argon-helium jets and may be beneficial for obtaining the desired performance in the plasma spraying process.

V. REFERENCES

1. E. Pfender, "Thermal plasma processing in the nineties", *Pure & Appl. Chem.*, 60, 590 (1988).
2. E. Pfender, R. Spores and W. L. T. Chen, "A new look at the thermal and gas dynamic characteristics of a plasma jet ",1990 National Thermal Spraying Conference, Long Beach, CA, May 21 - 24, 1990.
3. E. Pfender and Y. C. Lee, "Particle dynamics and particle heat and mass transfer in thermal plasma. Part I. The motion of a single particle without thermal effects ", *Plasma Chem. Plasma Process.*, 5, 211 (1985).
4. Y. C. Lee, Y. P. Chyou and E. Pfender, "Particle dynamics and particle heat and mass transfer in thermal plasma. Part II. Particle heat and mass transfer in thermal plasmas." *Plasma Chem. Plasma Process.*, 5, 391 (1985).
5. Y. C. Lee and E. Pfender, "Particle dynamics and particle heat and mass transfer in thermal plasma. Part III. Thermal plasma jet reactors and multiparticle injection", *Plasma Chem. Plasma Process.*, 7, 1 (1987).
6. Y. P. Chyou and E. Pfender, "Modeling of plasma jets with superimposed vortex flow", *Plasma Chem. Plasma Process.*, 9, 291 (1989).
7. M. Brossa and E. Pfender, "Probe measurements in thermal plasma jets", *Plasma Chem. Plasma Process.*, 8, 75 (1988).
8. A. Capetti and E. Pfender, "Probe measurements in argon plasma jets operated in ambient argon", *Plasma Chem. Plasma Process.*, 9, 329 (1989).

9. R. Spores and E. Pfender, "Flow structure of a turbulent thermal plasma jet", *Surface and Coating Technology*, 37, 251 (1989).
10. W. L. T. Chen and E. Pfender, "Two-dimensional temperature measurements in thermal plasma jets using an OMA system", High Temperature Laboratory, Department of Mechanical Engineering, University of Minnesota, December 1988.
11. W. L. T. Chen and E. Pfender, "Two-dimensional temperature measurements in thermal plasma jets using an OMA system", 9th International Symposium on Plasma Chemistry, Pugnochiuso, Italy, Sept. 1989, Vol. I, pp 330 - 335.
12. W. L. T. Chen and E. Pfender, "Enthalpy probe and spectroscopic measurements in thermal plasma jets", Center for Plasma-Aided Manufacturing, Department of Mechanical Engineering, University of Minnesota, April 1990.
13. W. L. T. Chen, J. Heberlein and E. Pfender, "Experimental measurements of plasma properties for Miller SG-100 torch with Mach I setting. Part 1. Enthalpy probe measurements", Center for Plasma-Aided Manufacturing, Department of Mechanical Engineering, University of Minnesota, August 1990.
14. W. L. T. Chen, J. Heberlein and E. Pfender, "Experimental measurements of plasma properties for Miller SG-100 torch with Mach I setting. Part 2. Spectroscopic measurements and comparisons with enthalpy probe data", Center for Plasma-Aided Manufacturing, Department of Mechanical Engineering, University of Minnesota, September 1990.
15. A. T. Hattenburg, "Spectral radiance of a low current graphite arc", *Applied Optics*, 6, 95 (1967).

16. C. D. Maldonado, A.P. Carm and H. N. Olsen, "New method for obtaining emission coefficients from emitted spectral intensities. Part I Circularly symmetric light sources", *J. Opt. Soc. Am.*, 55, 1274 (1965).
17. J. B. Tatum and W. A. Jaworski, "A solution of Abel's equation", *J. Quant. Spectrosc. Radiat. Transfer*, 38, 319 (1987).
18. K. C. Hsu, "A self consistent model for the high intensity free-buring arc", Ph.D. Thesis, University of Minnesota, 1982.
19. Y. C. Lee, "Modeling work in plasma processing", Ph.D. Thesis, University of Minnesota, 1984.
20. E. Schulz-Gulde, "The continuous emission of argon in the visible spectral range ", *Z. Physik*, 230, 449 (1970).
21. W. L. Wiese, "The atomic transition probabilities of argon — a continuing challenge to plasma spectroscopy", *J. Quant. Spectrosc. Radiat. Transfer*, 40, 421 (1988).
22. R. C. Preston, "Spectroscopic studies of a plasma temperature and radiation standard based on a wall-stabilized arc", *J. Quant. Spectrosc. Radiat. Transfer*, 18, 337 (1977).
23. J. Mostaghimi, "Comments on the use of water cooled probes for velocity measurements in thermal plasma flows", private communication, Oct. 1988.
24. C. Boffa, J. Heberlein and E. Pfender, "Criterion for establishing deviation from the local thermodynamic equilibrium in atmospheric pressure plasma jets", *Wärme- und Stoffübertragung*, 4, 213 (1971).
25. W. L. T. Chen , "Theoretical calculation of LTE plasma properties in argon-helium thermal plasma of 1 atm pressure", Center for Plasma-Aided Manufacturing, Department of Mechanical Engineering, University of Minnesota, June 1990.

26. C. P. Chiu, Written Prelim, A report for Dr. Pfender, July 2, 1990.

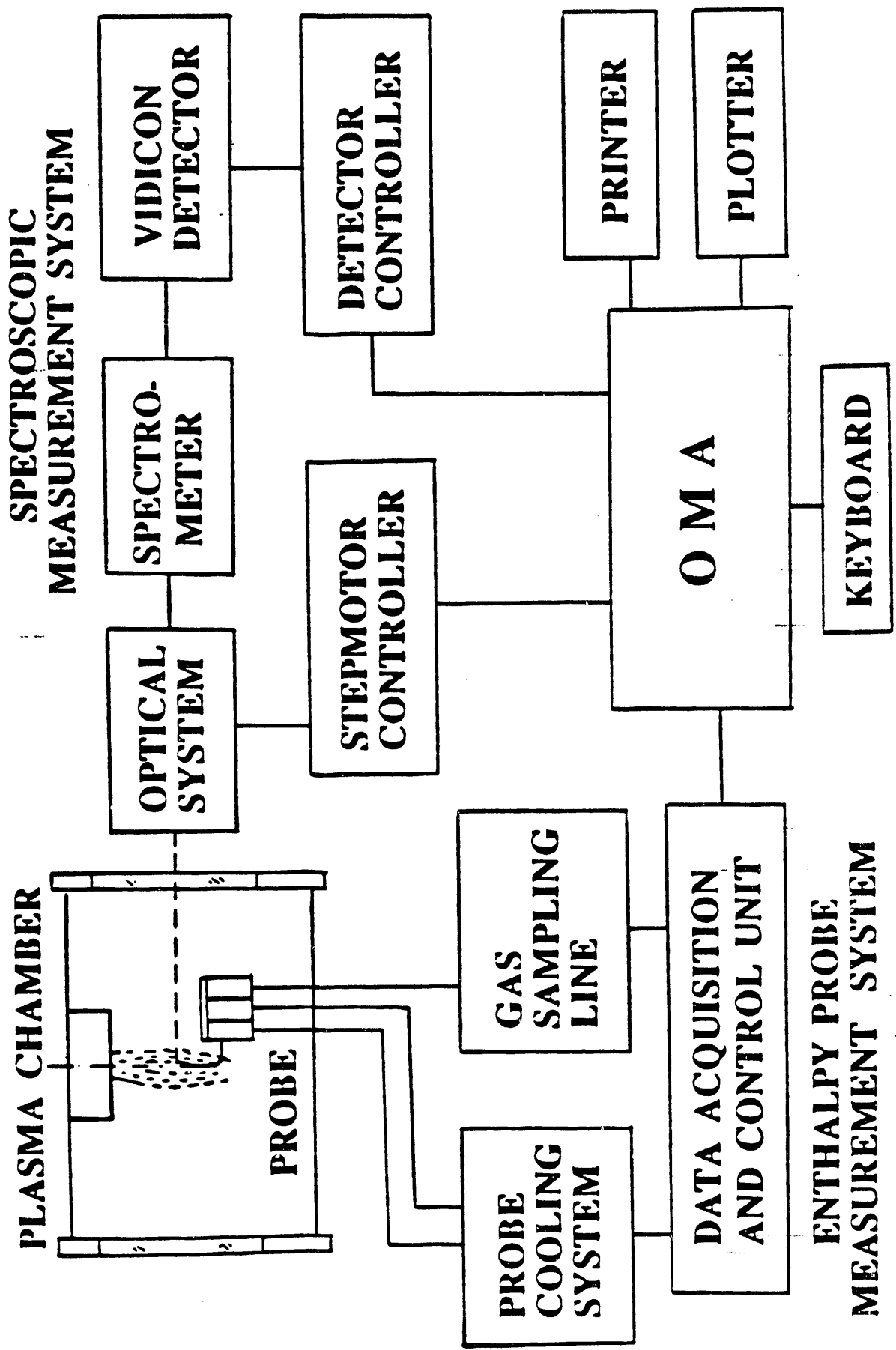
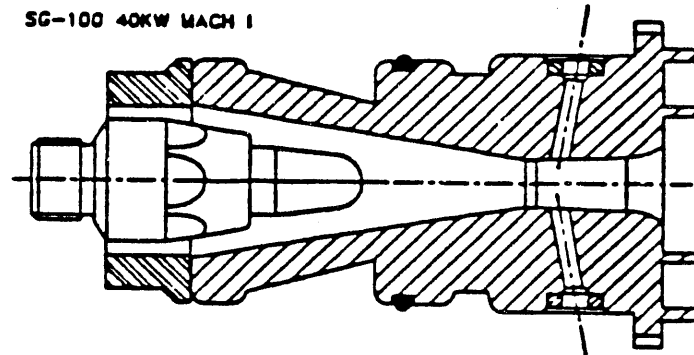


Fig. 1 Schematic of the integral experimental set-up.

Miller SG-100 Mach I Plasma Gun



Anode	2083-155
Cathode	1083A-112
Gas Injector	1083A-113
Argon-Helium Gas Flow Rate	1 Atm Ar: 100 SCFH He: 47 SCFH
Current	800 A
Voltage	38 V
Efficiency	58.4 %

Fig. 2 Miller SG-100 Mach I plasma gun.

VIDICON
SPECTROMETER
DETECTOR

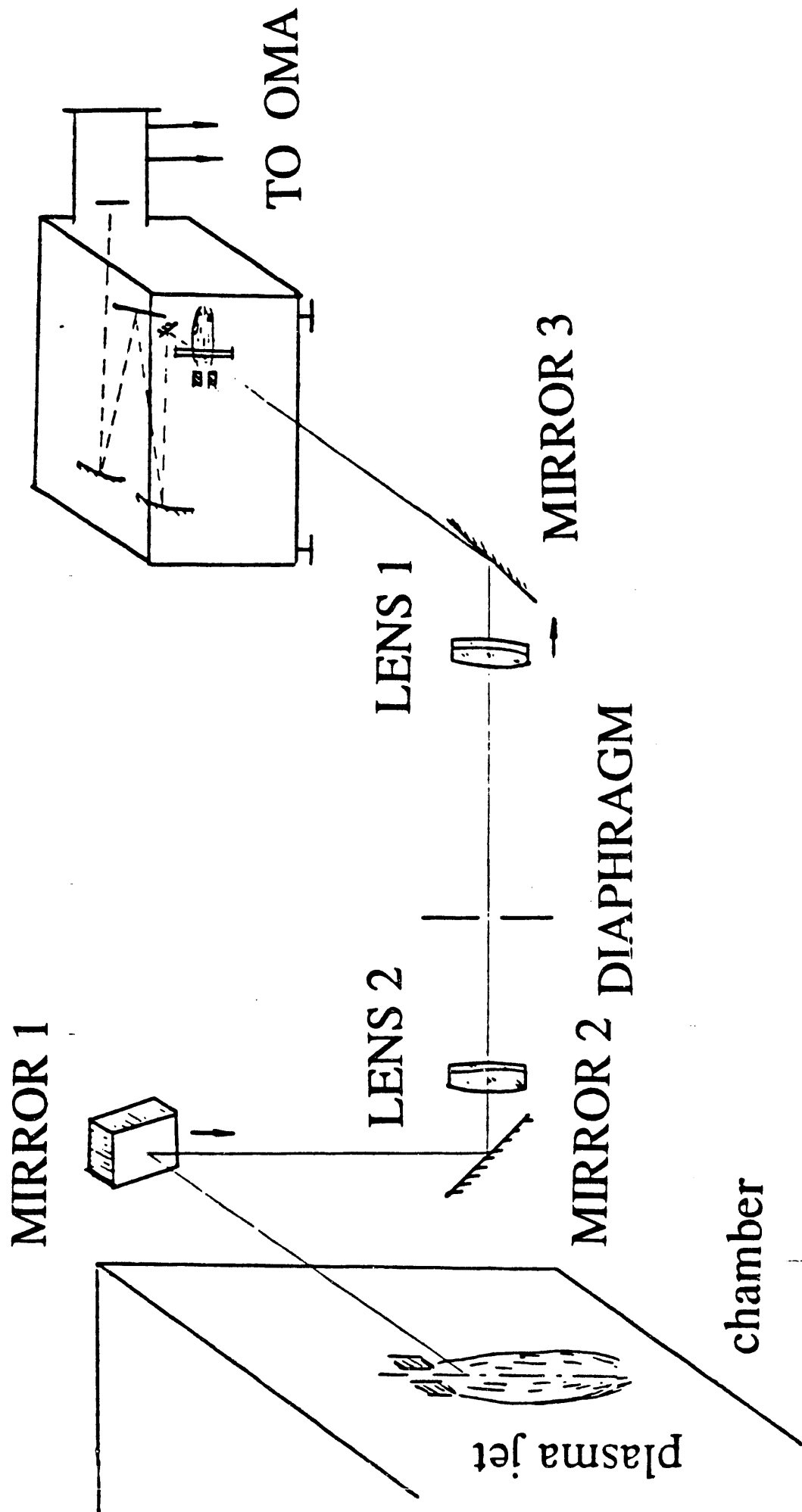


Fig. 3 Optical system for spectrometric measurements.

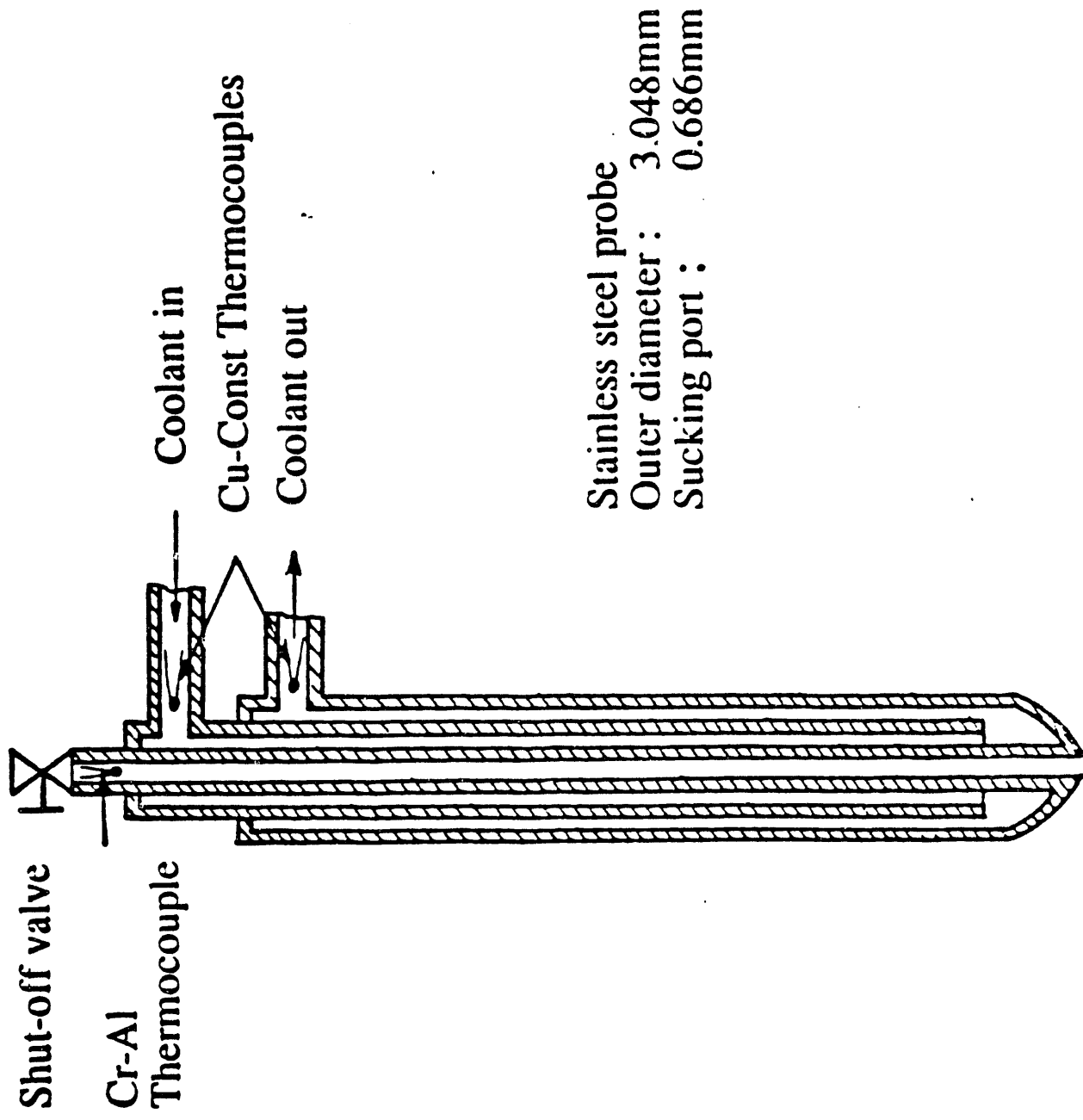


Fig. 4 Schematic of enthalpy probe.

P - Piezoresistive pressure transducers

T - Chromel-Alumel thermocouples

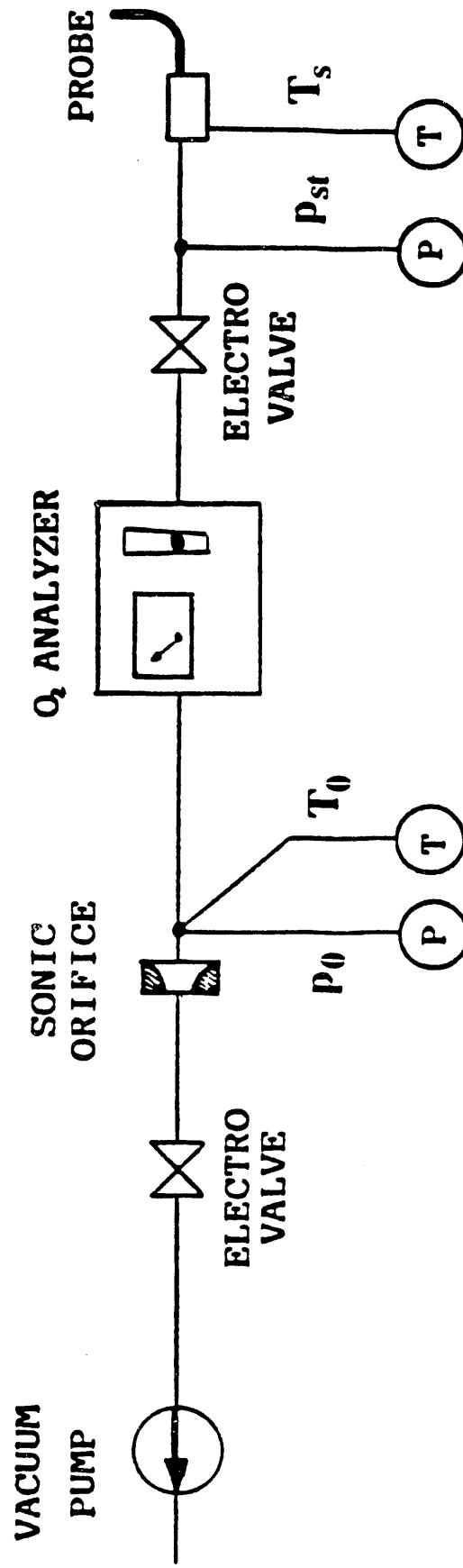


Fig. 5 Gas sampling line for enthalpy probe measurements.

I=800A
Ar: 100 SCFH
He: 47 SCFH

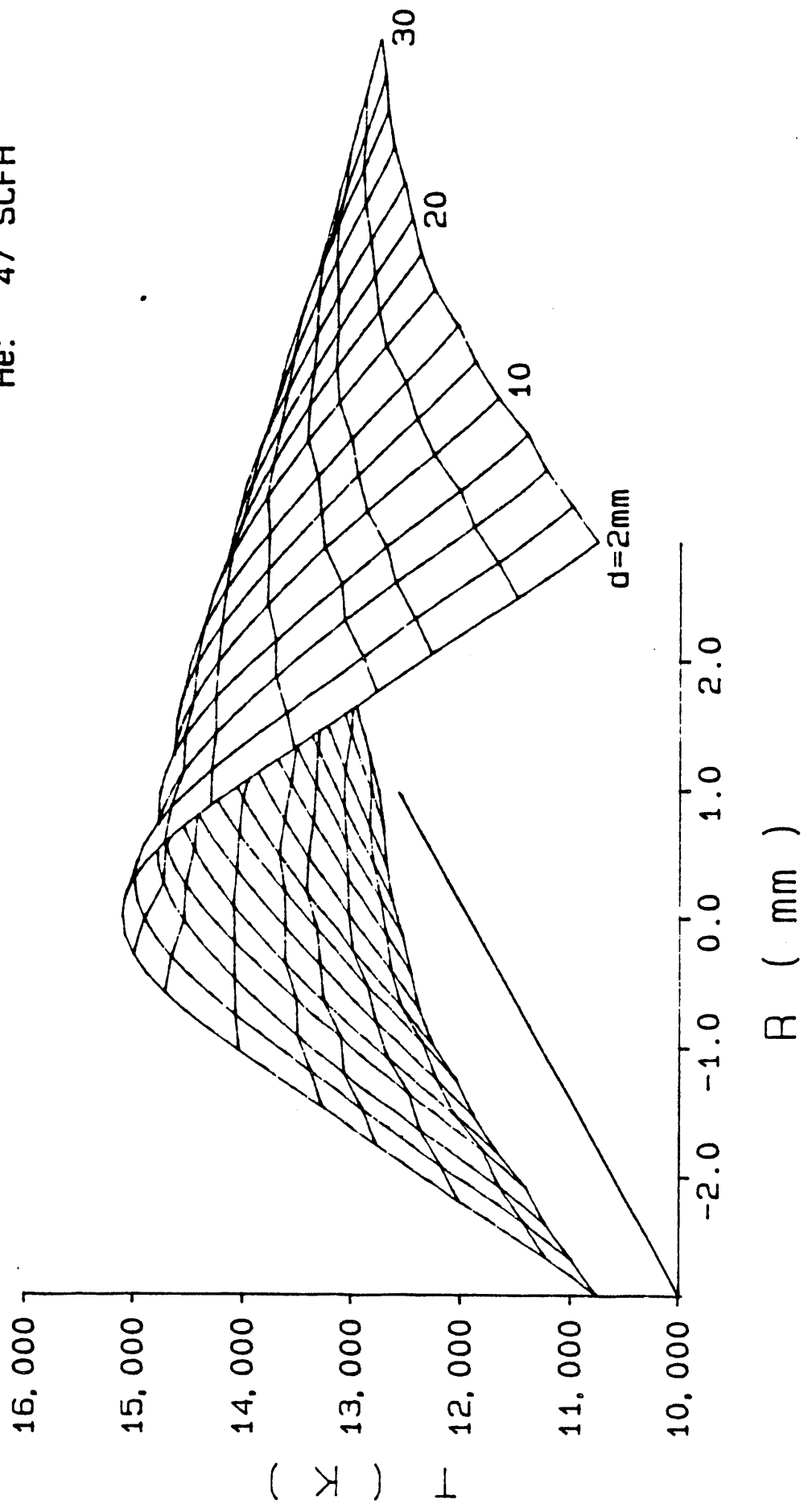


Fig. 6 Temperature profiles, plotted as a three-dimensional pattern, derived from spectroscopic measurements.

Measurement region: $d = 2 \text{ mm} - 30 \text{ mm}$. ($d =$ distance from nozzle exit)

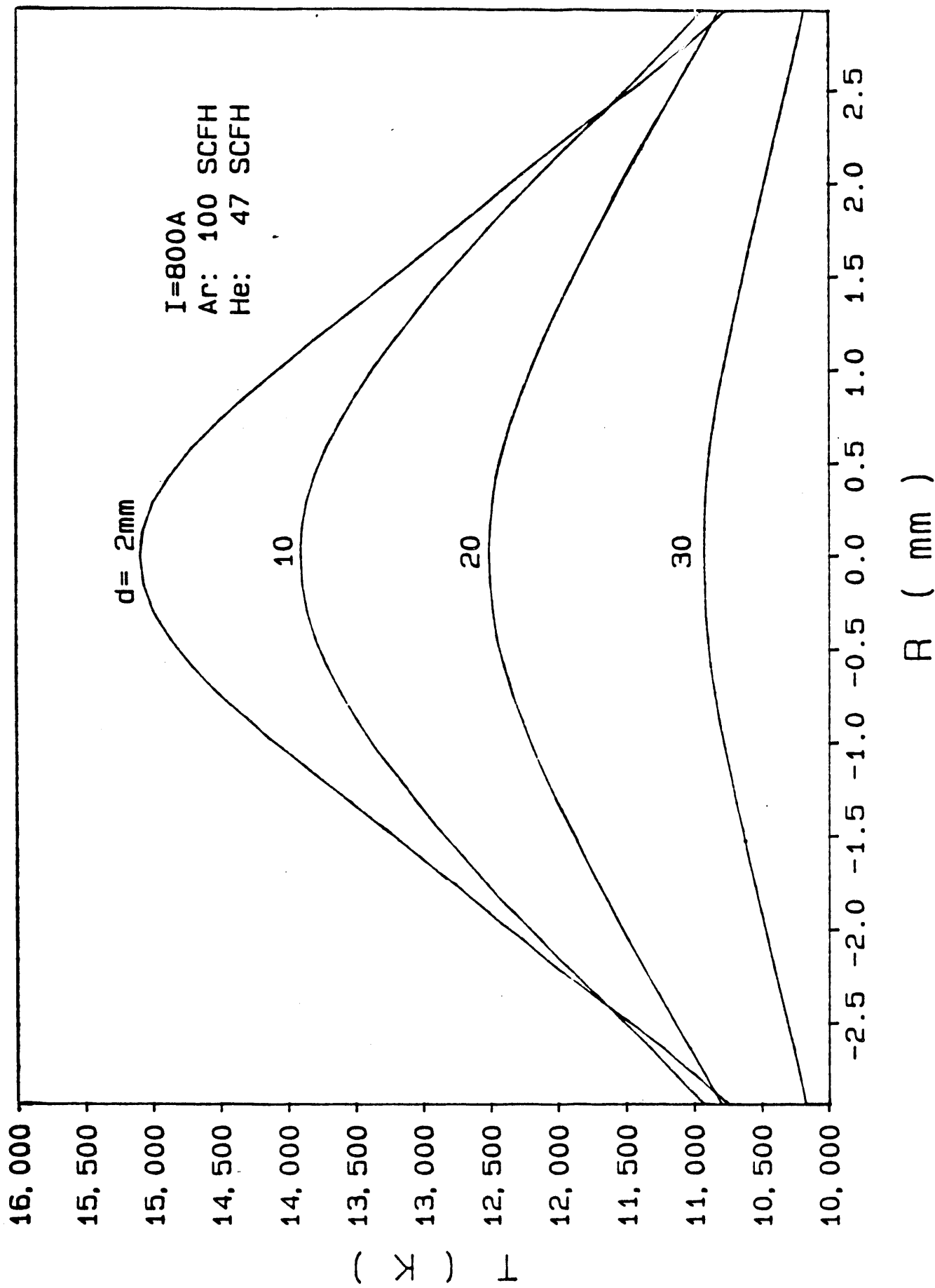


Fig. 7 Temperature profiles, plotted as a two-dimensional pattern, derived from spectroscopic measurements.
 Measurement region: d = 2 mm - 30 mm. (d = distance from nozzle exit)

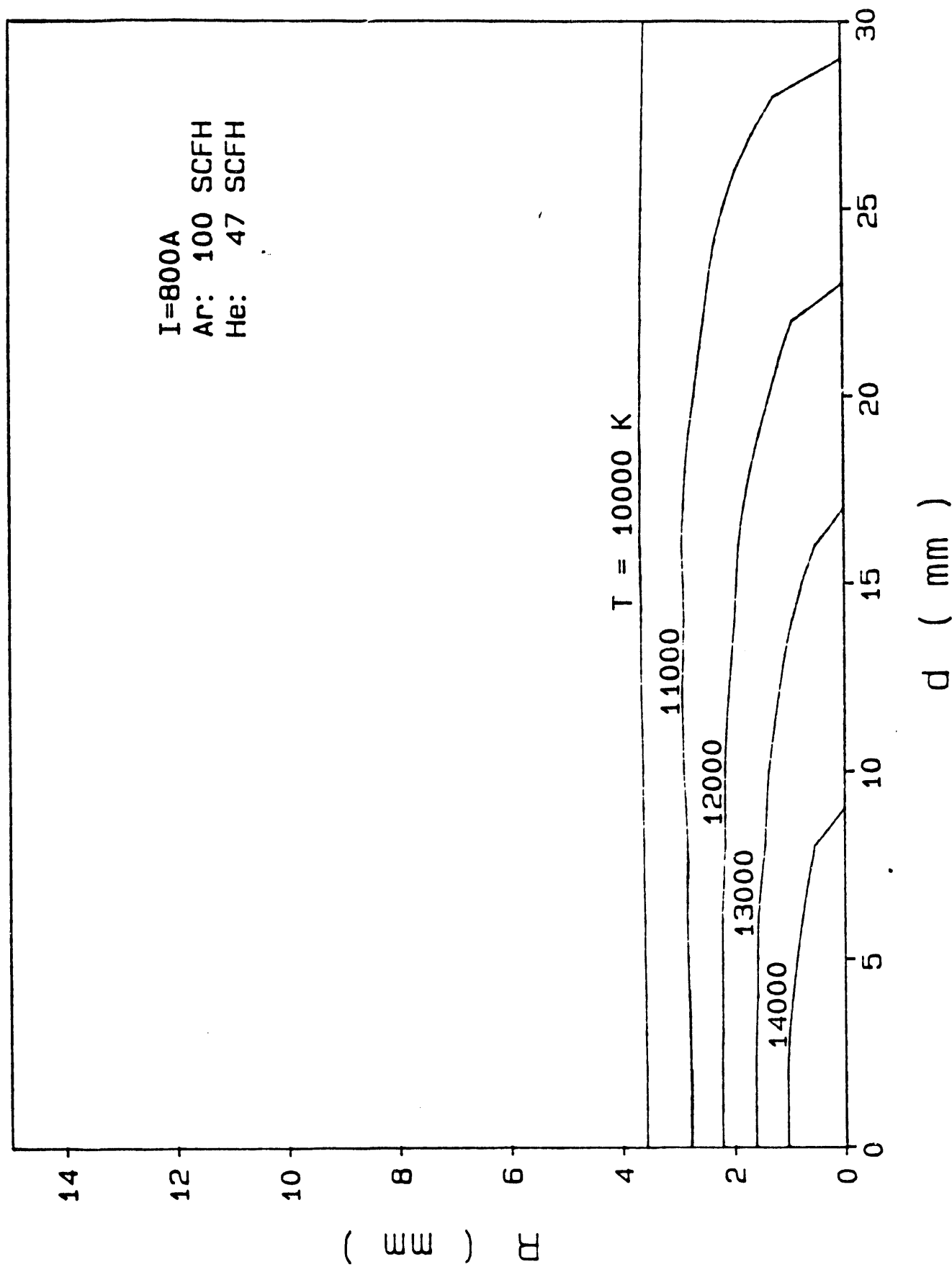


Fig. 8 Isotherms derived from spectroscopic measurements.

Measurement region: $d = 2 \text{ mm} - 30 \text{ mm}$. ($d = \text{distance from nozzle exit}$)

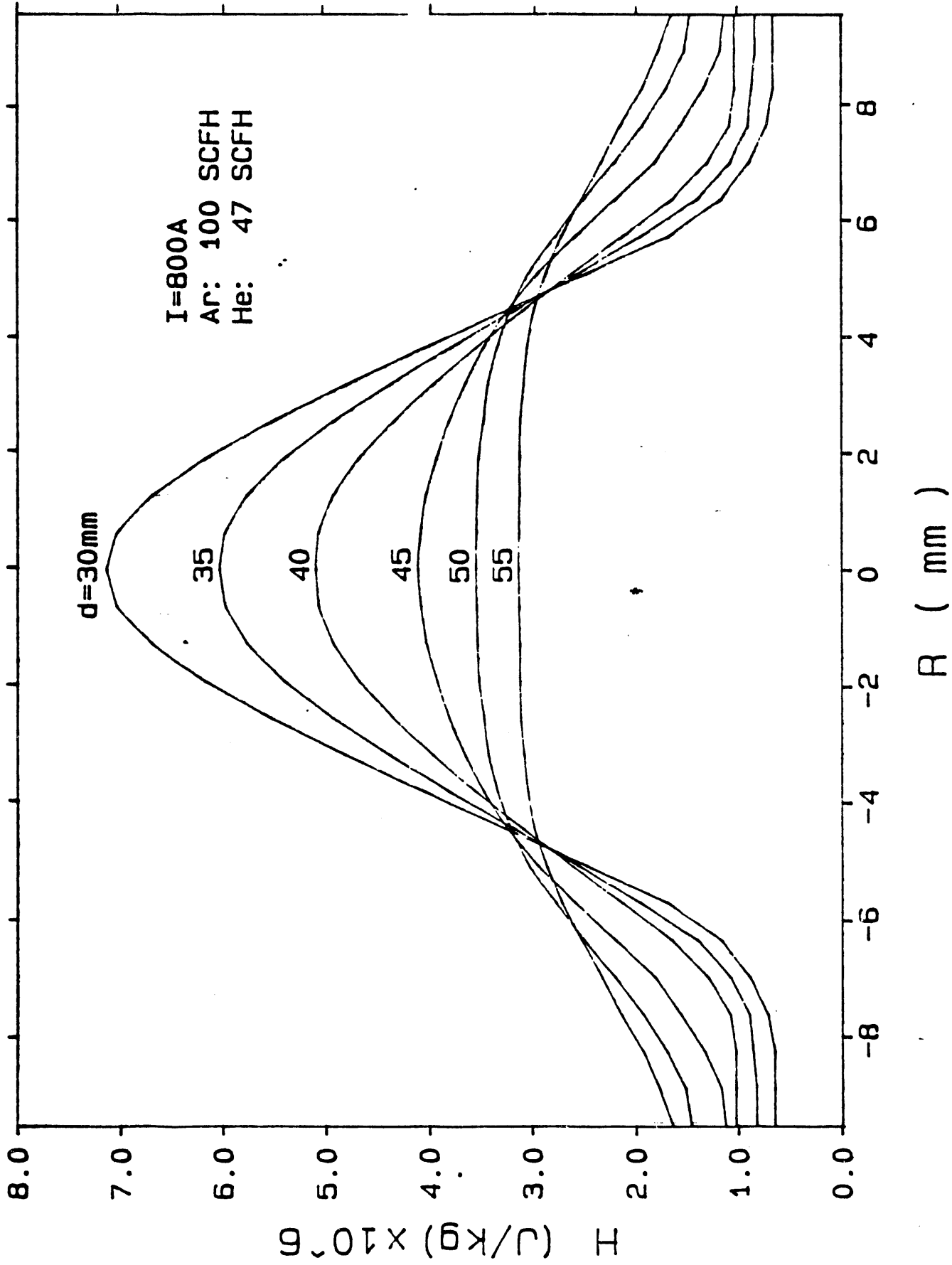


Fig. 9 Enthalpy profiles, plotted as a two-dimensional pattern.

Measurement region: $d = 30$ mm - 55 mm. ($d =$ distance from nozzle exit)

I=800A
Ar: 100 SCFH
He: 47 SCFH

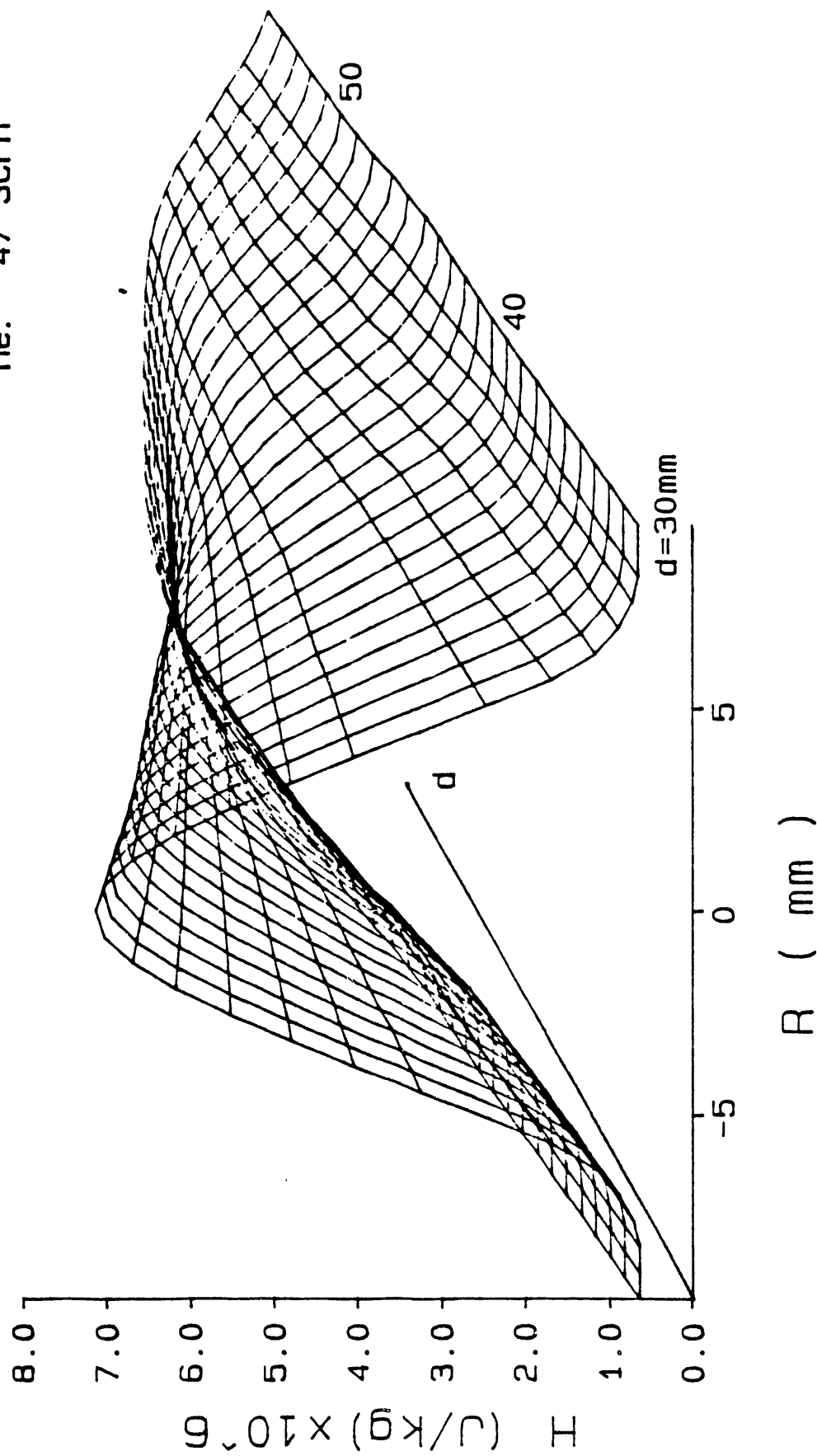


Fig. 10 Enthalpy profiles, plotted as a three-dimensional pattern.

Measurement region: $d = 30 \text{ mm} - 55 \text{ mm}$. ($d = \text{distance from nozzle exit}$)

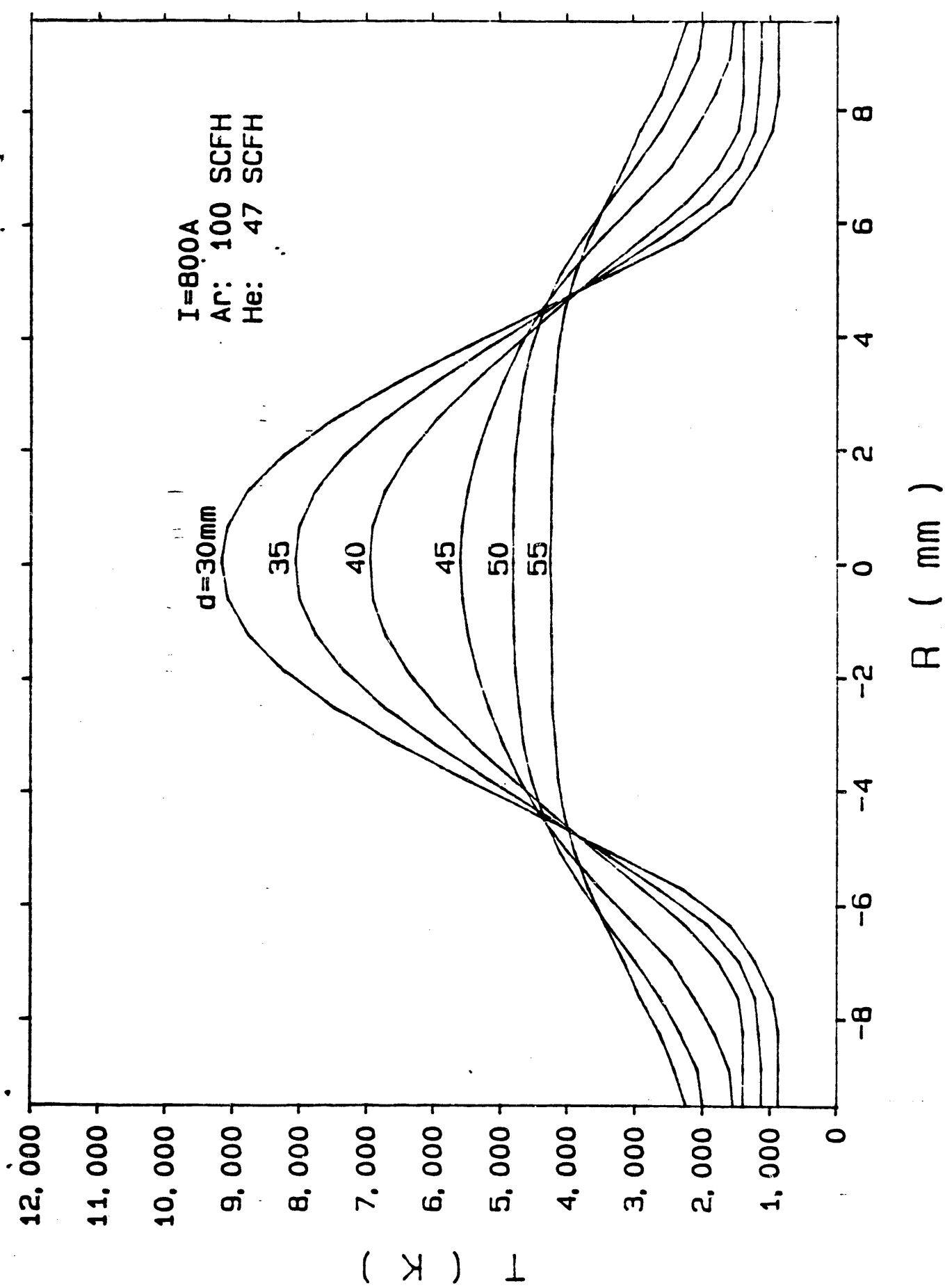


Fig. 11 Temperature profiles, plotted as a two-dimensional pattern, derived from enthalpy probe measurements. Measurement region: $d = 30 \text{ mm} - 55 \text{ mm}$. ($d = \text{distance from nozzle exit}$)

I=800A
Ar: 100 SCFH
He: 47 SCFH

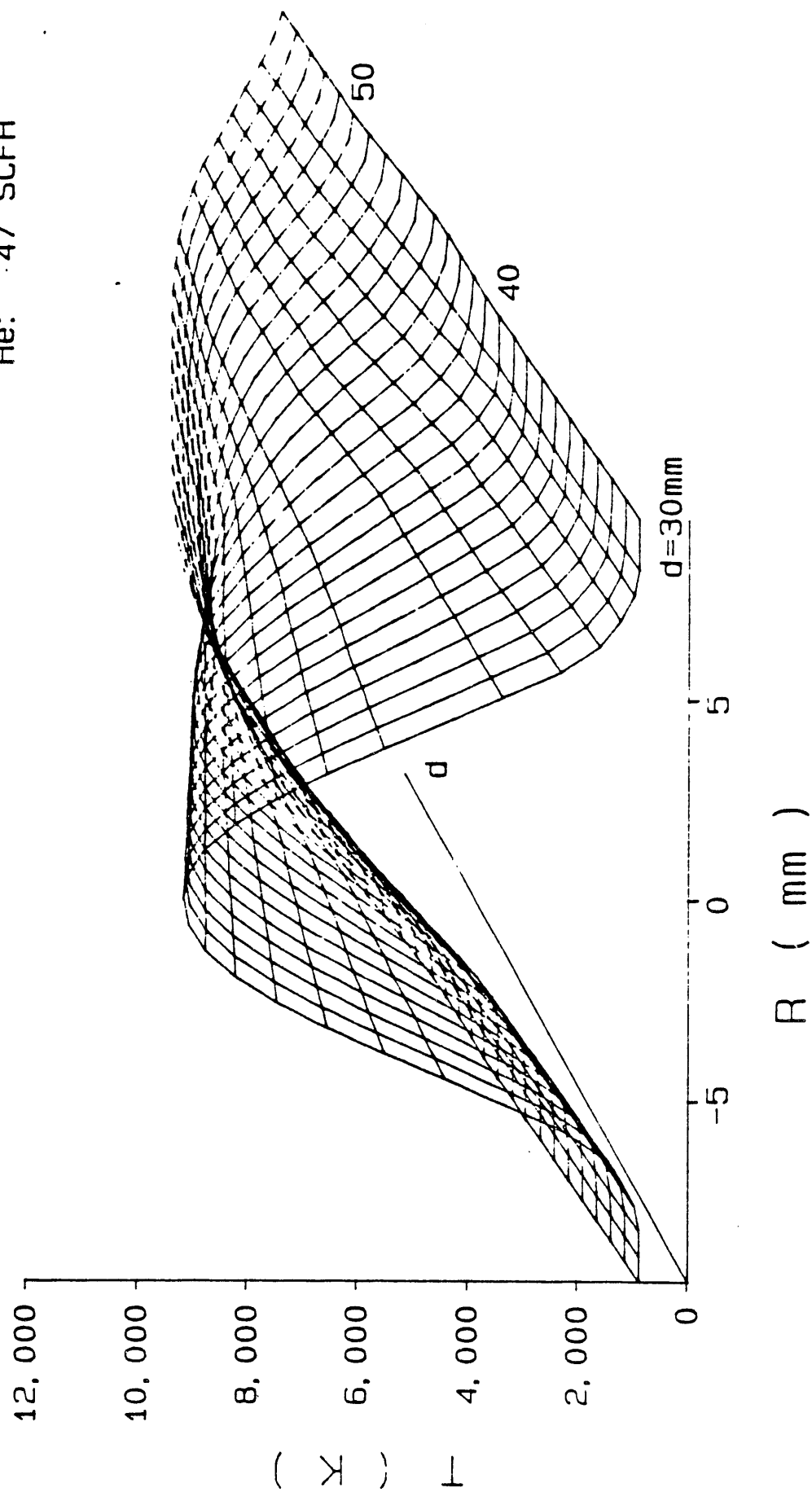


Fig. 12 Temperature profiles, plotted as a three-dimensional pattern, derived from enthalpy probe measurements.

Measurement region: $d = 30 \text{ mm} - 55 \text{ mm}$. ($d =$ distance from nozzle exit)

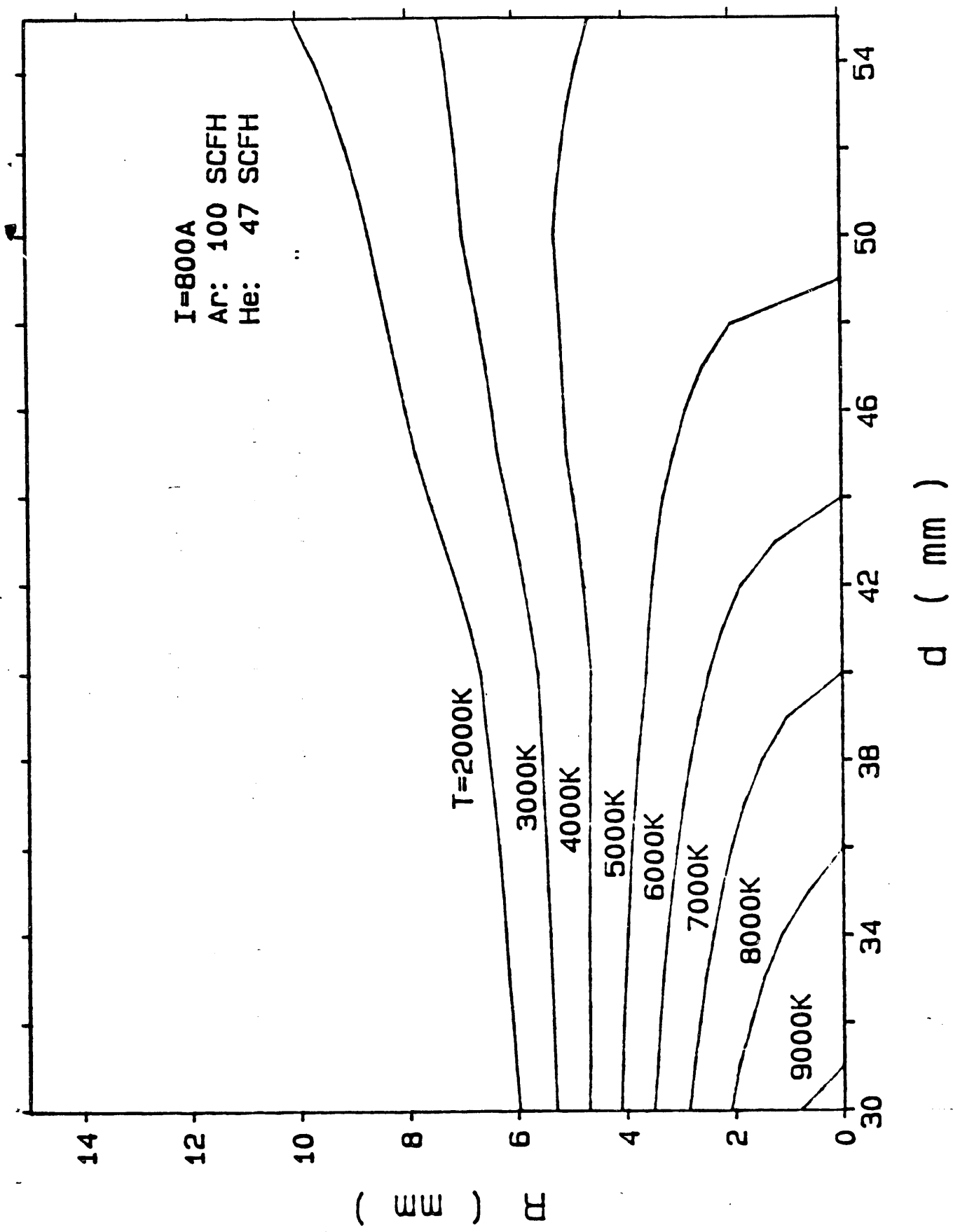


Fig. 13 Isotherms derived from enthalpy probe measurements..

Measurement region: d = 30 mm - 55 mm. (d = distance from nozzle exit)

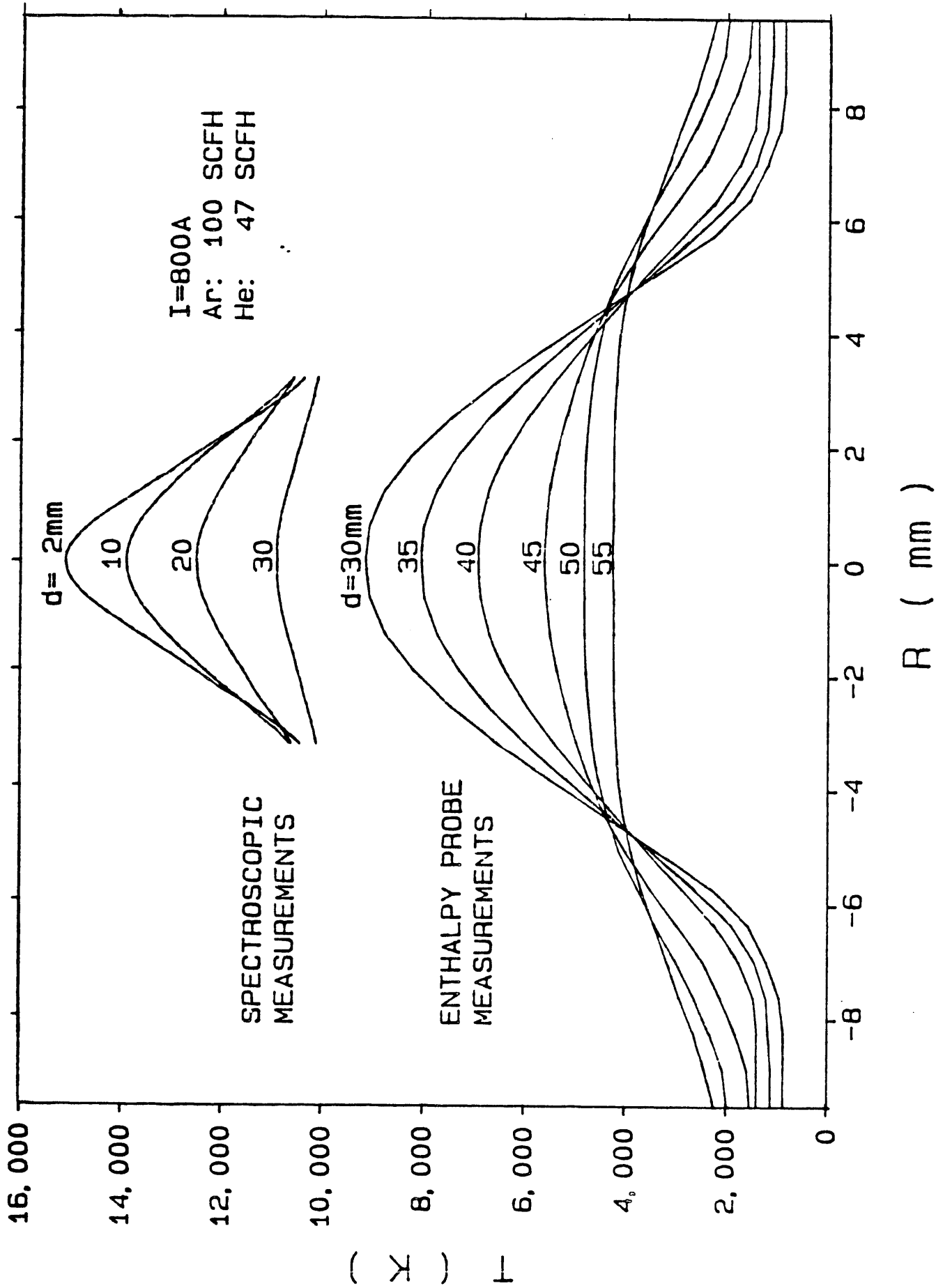


Fig. 14 Temperature profiles derived from spectroscopic and enthalpy probe measurements.
 Measurement region: $d = 2 \text{ mm} - 55 \text{ mm}$. ($d =$ distance from nozzle exit)

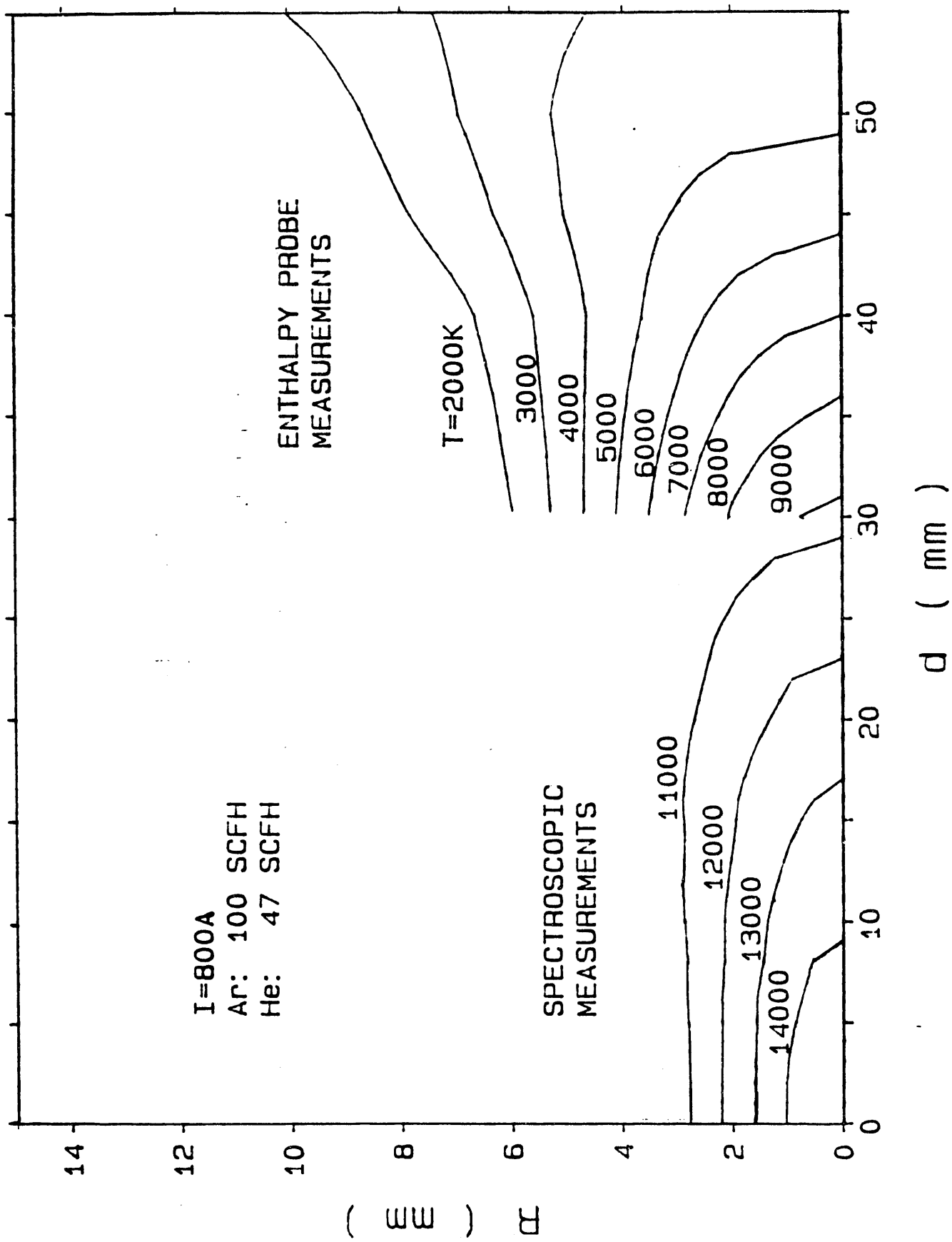


Fig. 15 Isotherms derived from spectroscopic and enthalpy probe measurements.
 Measurement region: $d = 2 \text{ mm} - 55 \text{ mm}$. (d = distance from nozzle exit)

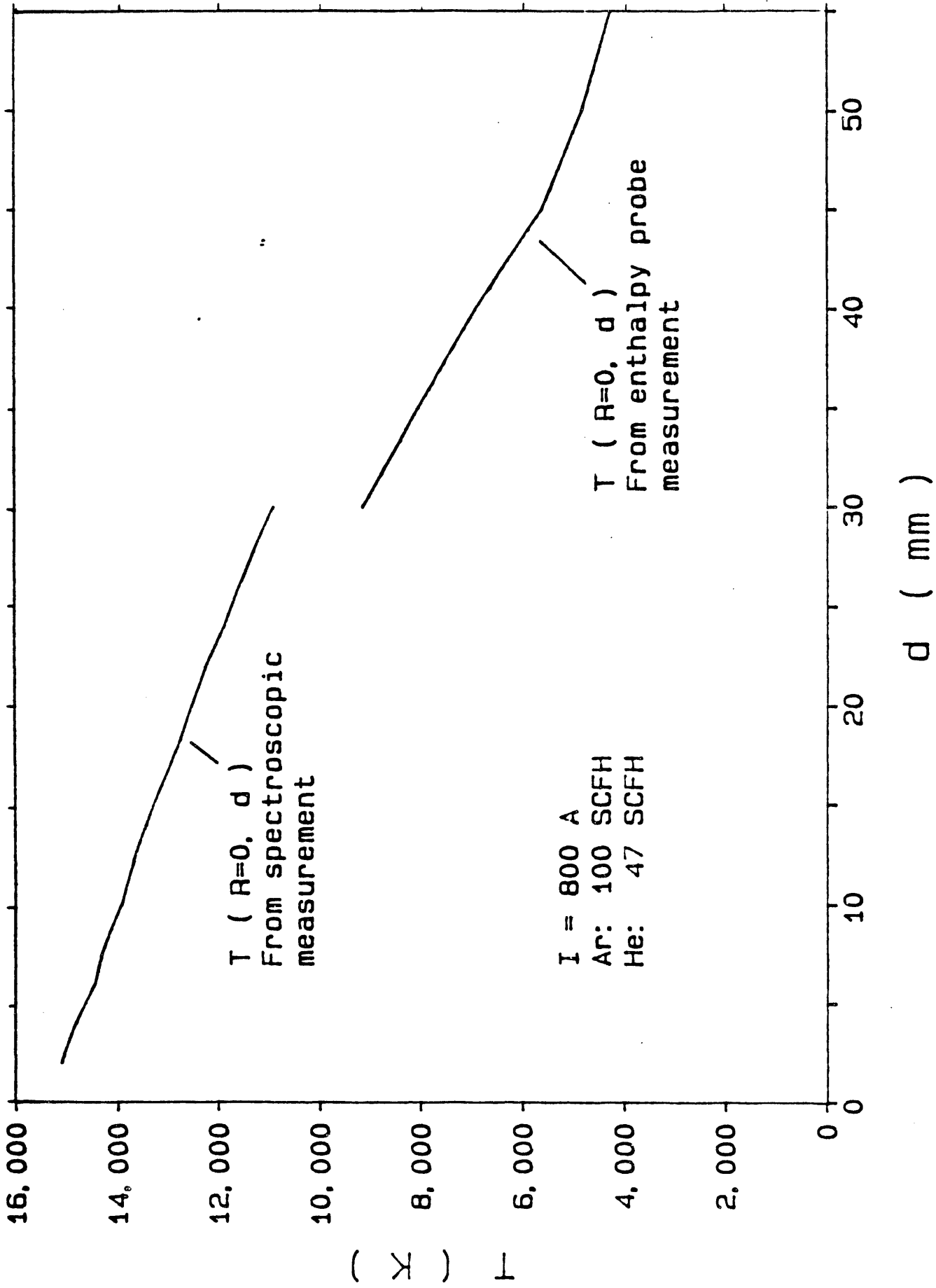


Fig. 16 Axial decay of temperature along the centerline of plasma jet.

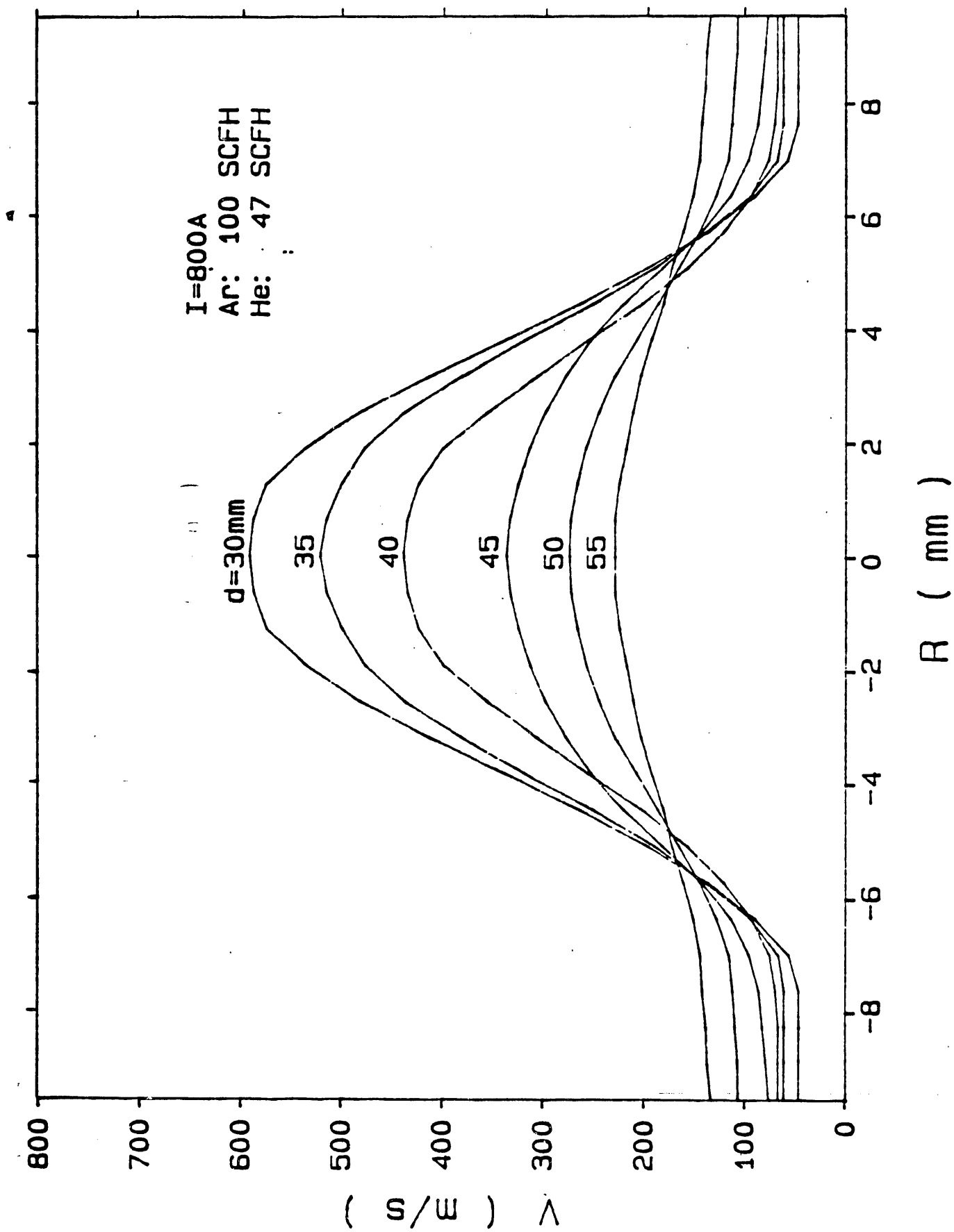


Fig. 17 Velocity profiles, plotted as a two-dimensional pattern.

I=800A
Ar: 100 SCFH
He: 47 SCFH

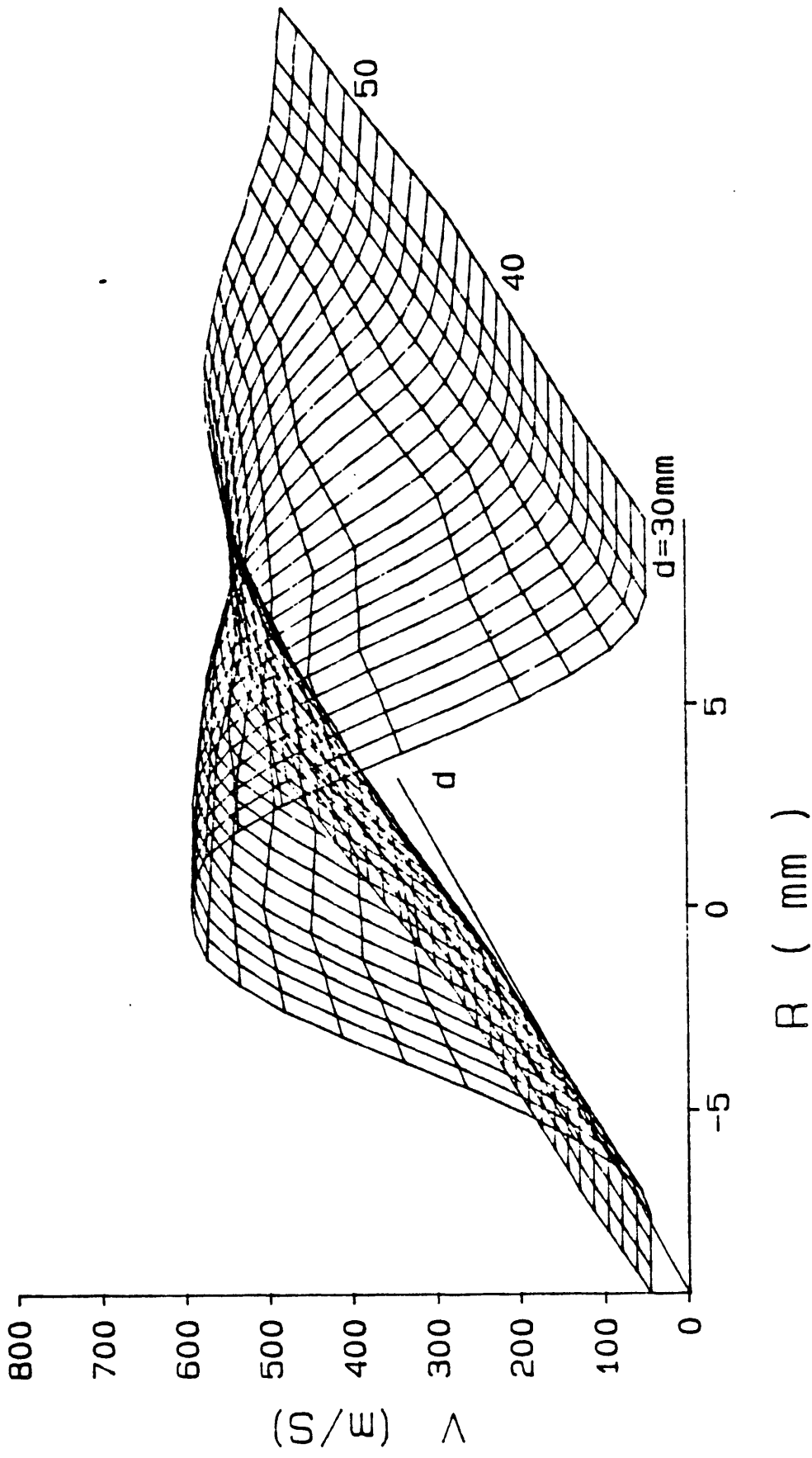


Fig. 18 Velocity profiles, plotted as a three-dimensional pattern.

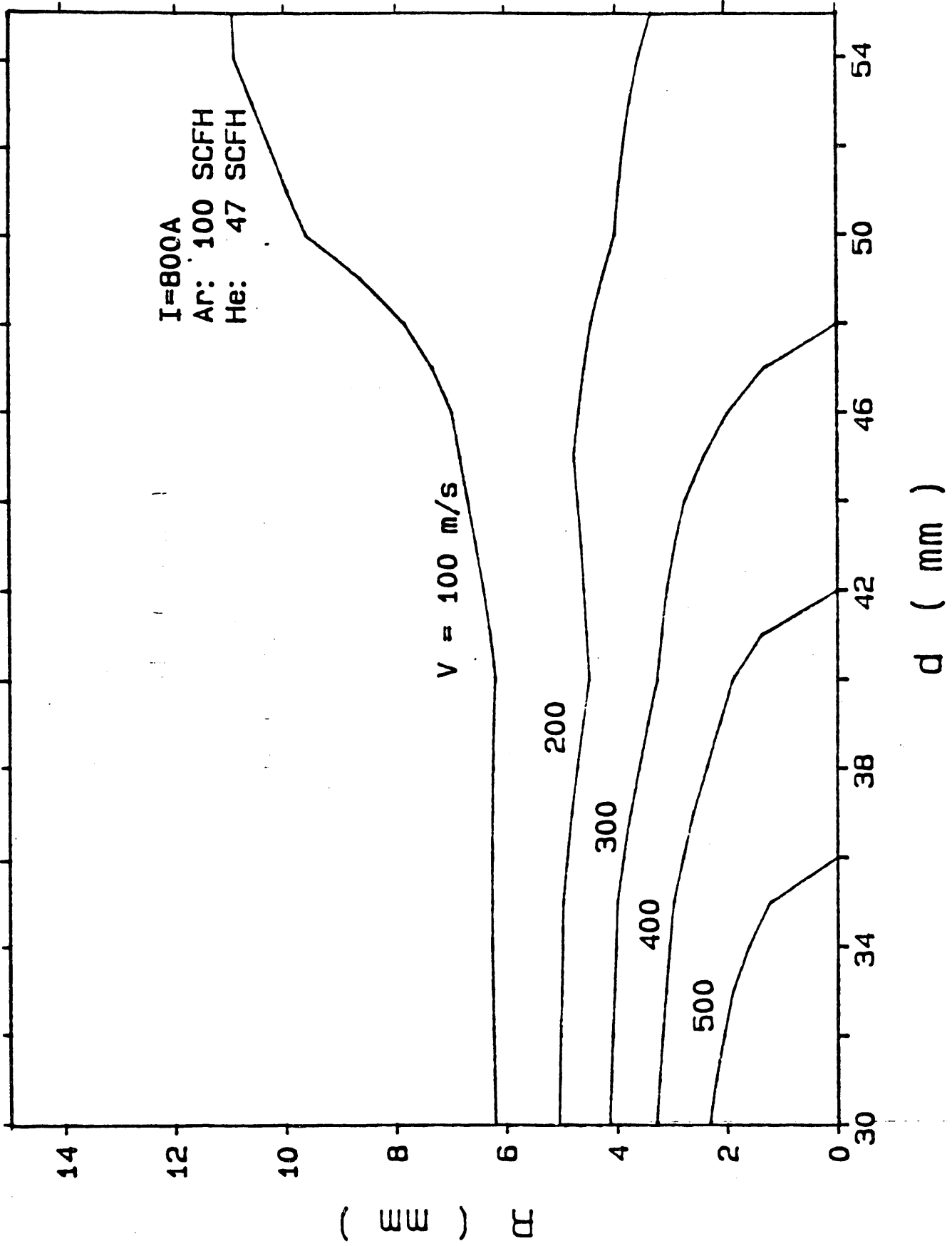


Fig. 19 Velocity isocontours.

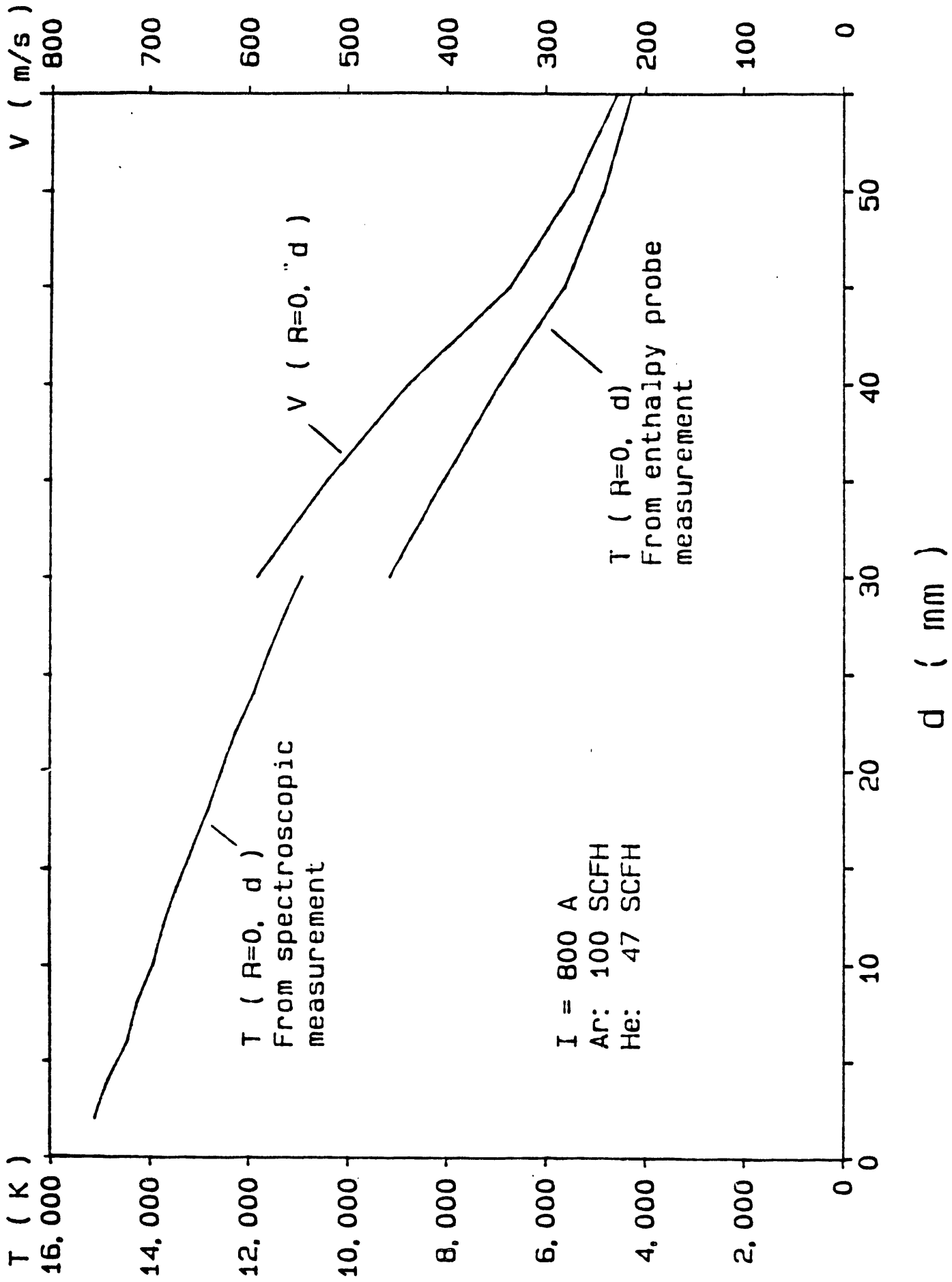


Fig. 20 Axial decay of temperature and of velocity along the centerline of plasma jet.

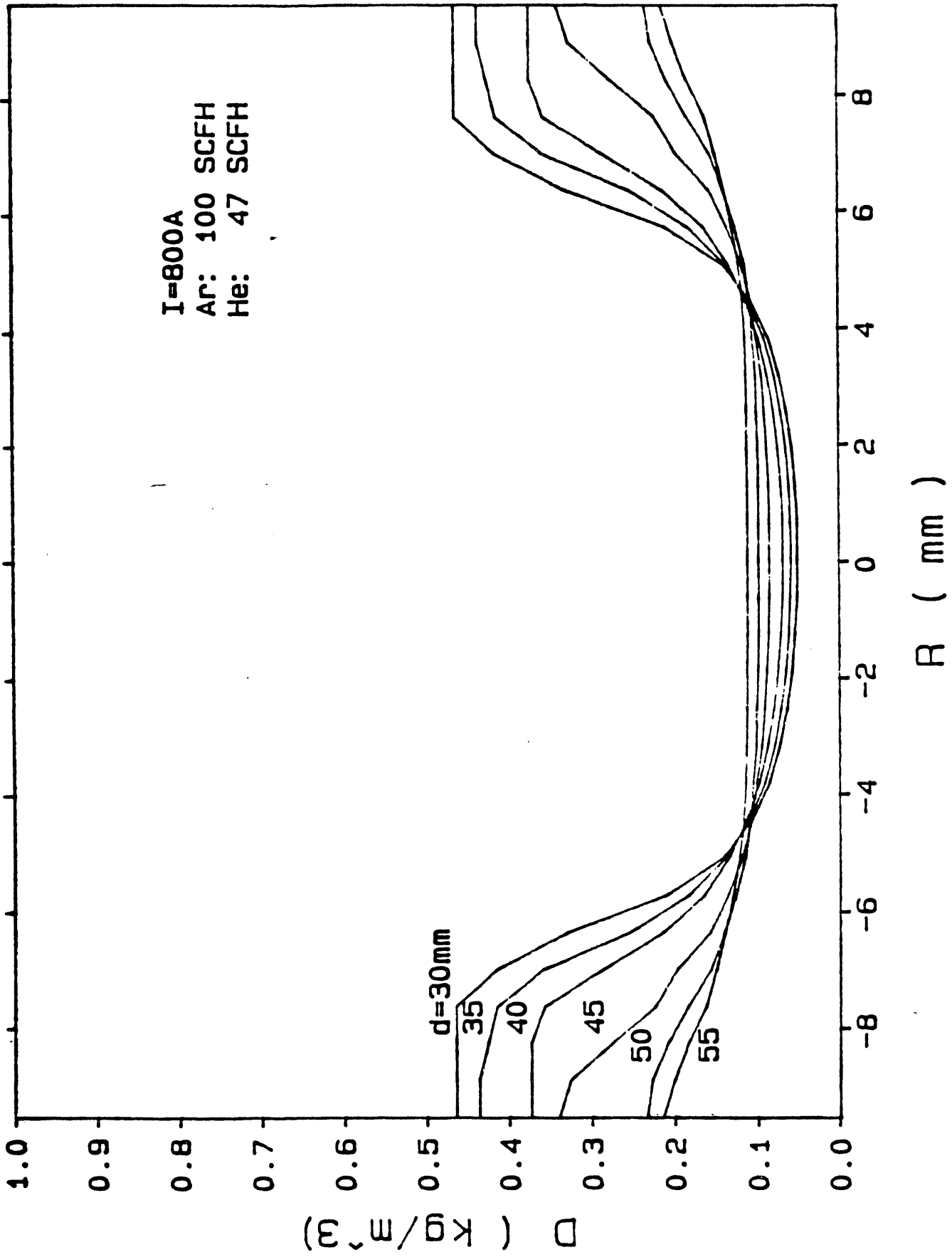


Fig. 21 Mass density profiles.

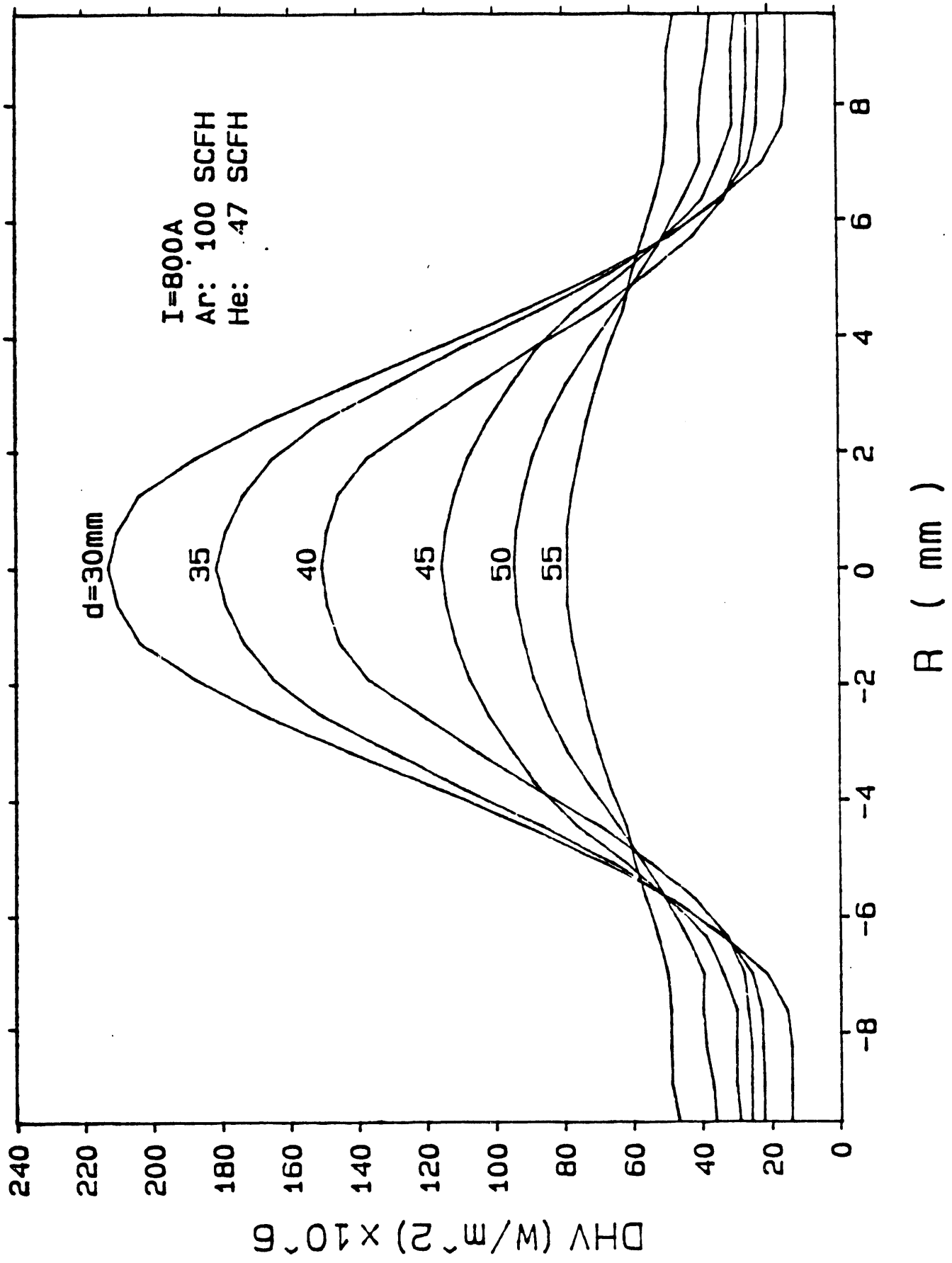


Fig. 22 Energy flux profiles.

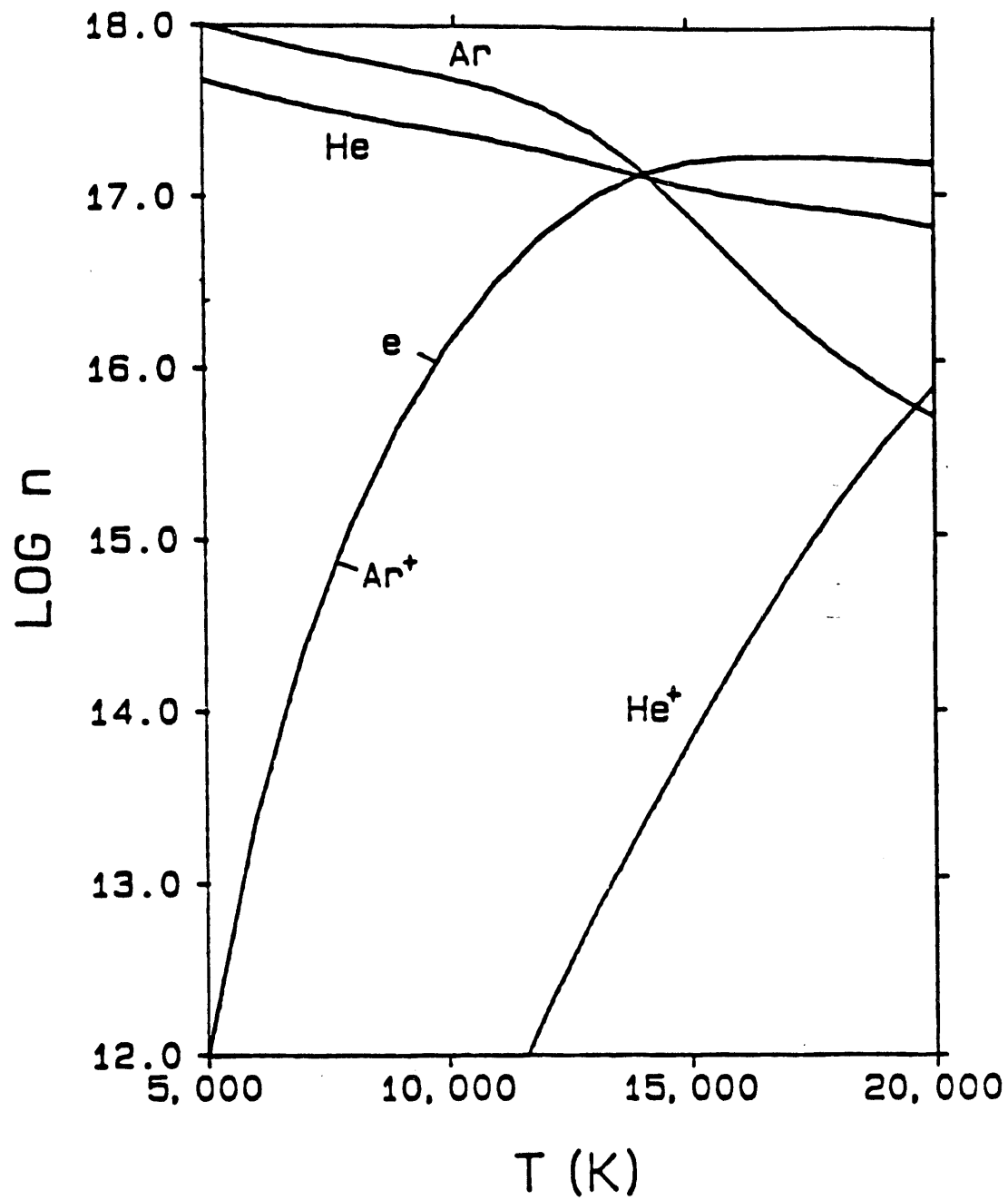


Fig. 23 Number densities of particles (unit in cm^{-3}) in argon-helium (100 : 47) thermal plasma of atmospheric pressure at different temperatures.

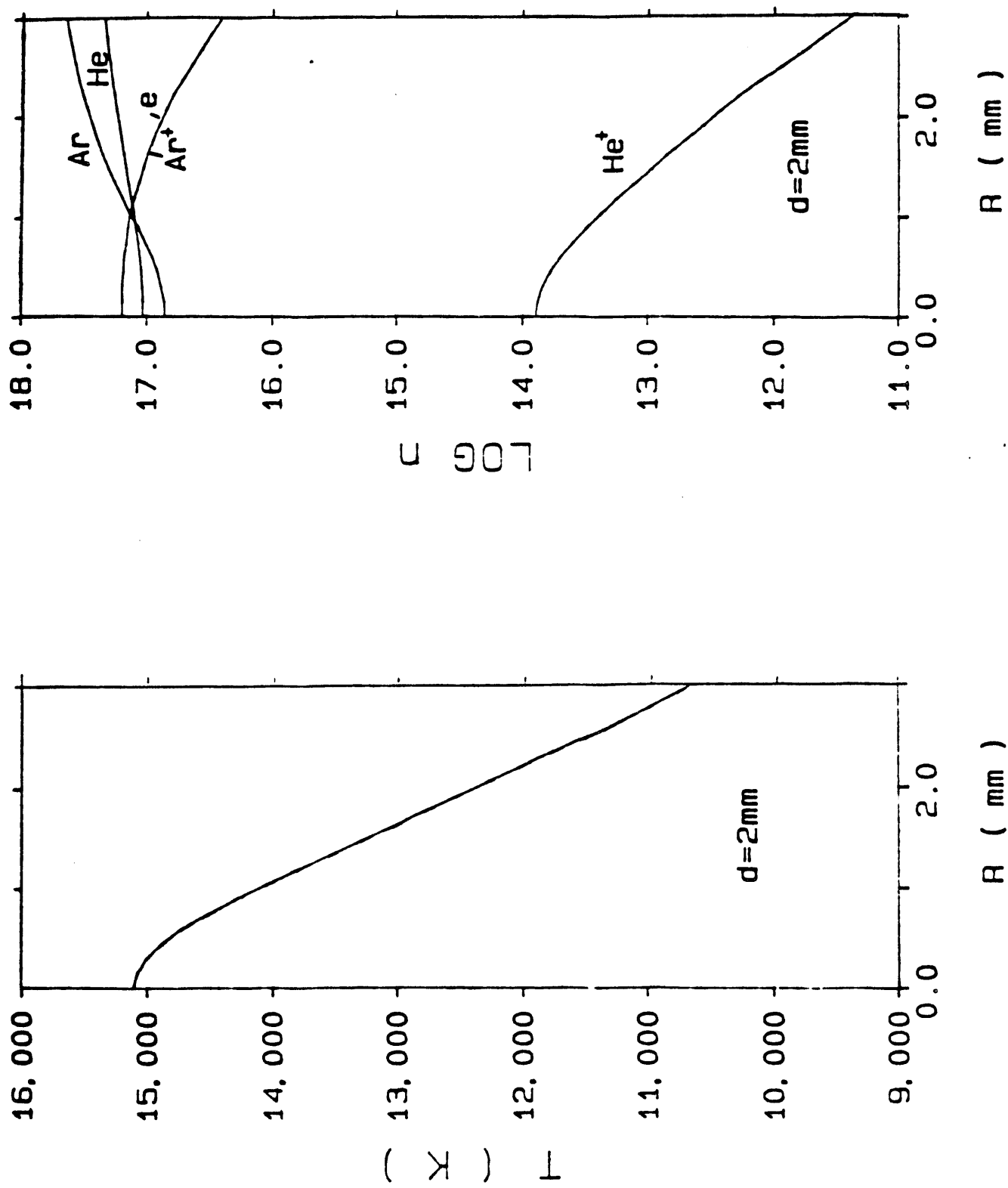


Fig. 24 Temperature and plasma composition profiles assuming LTE and derived from spectroscopic measurements ($d = 2mm$).

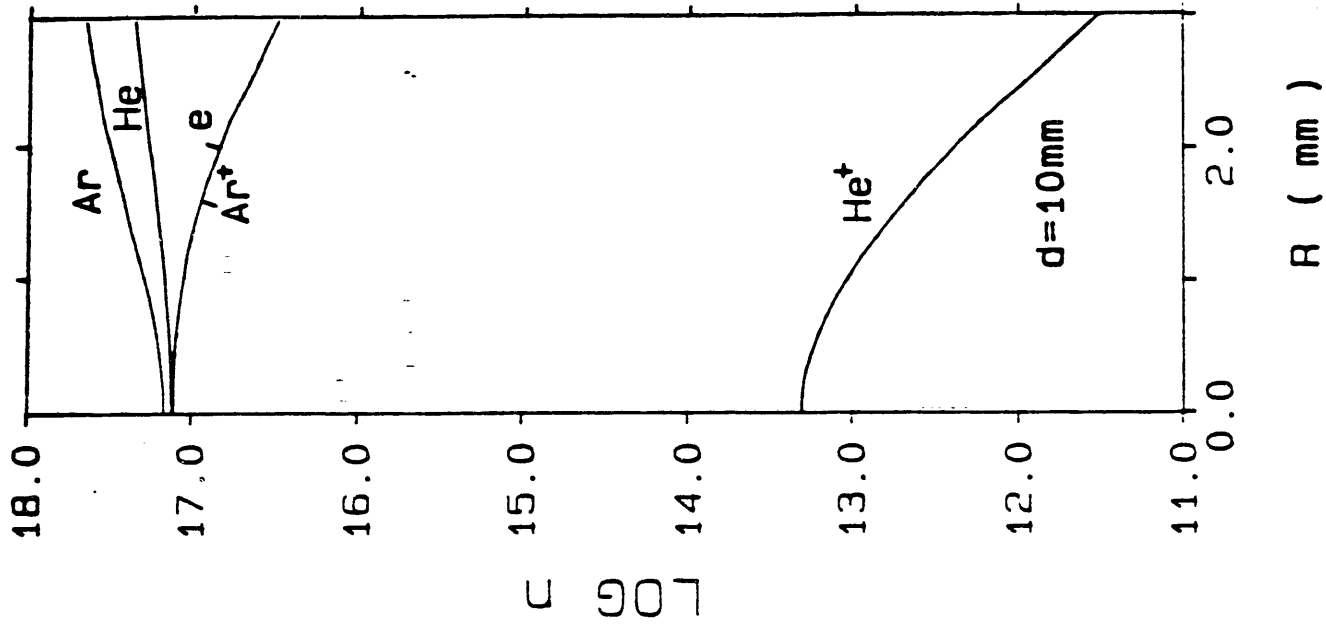
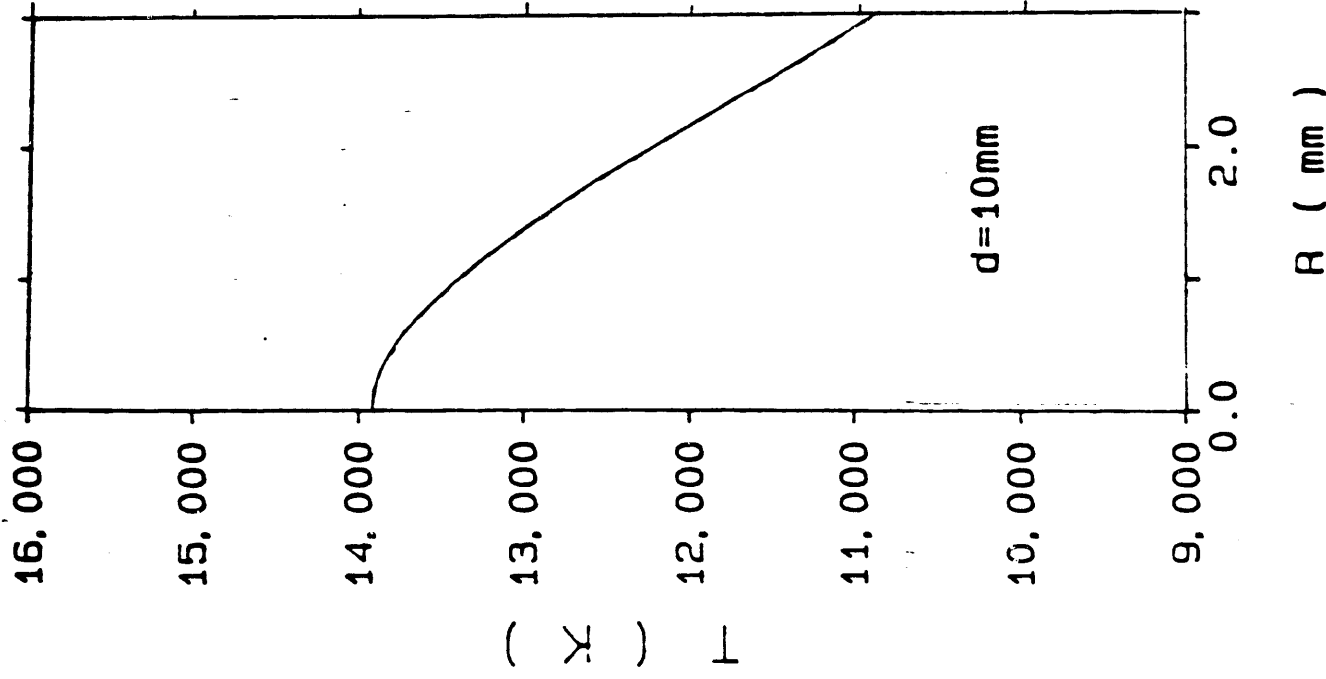


Fig. 25 Temperature and plasma composition profiles assuming LTE and derived from spectroscopic measurements ($d = 10\text{mm}$).

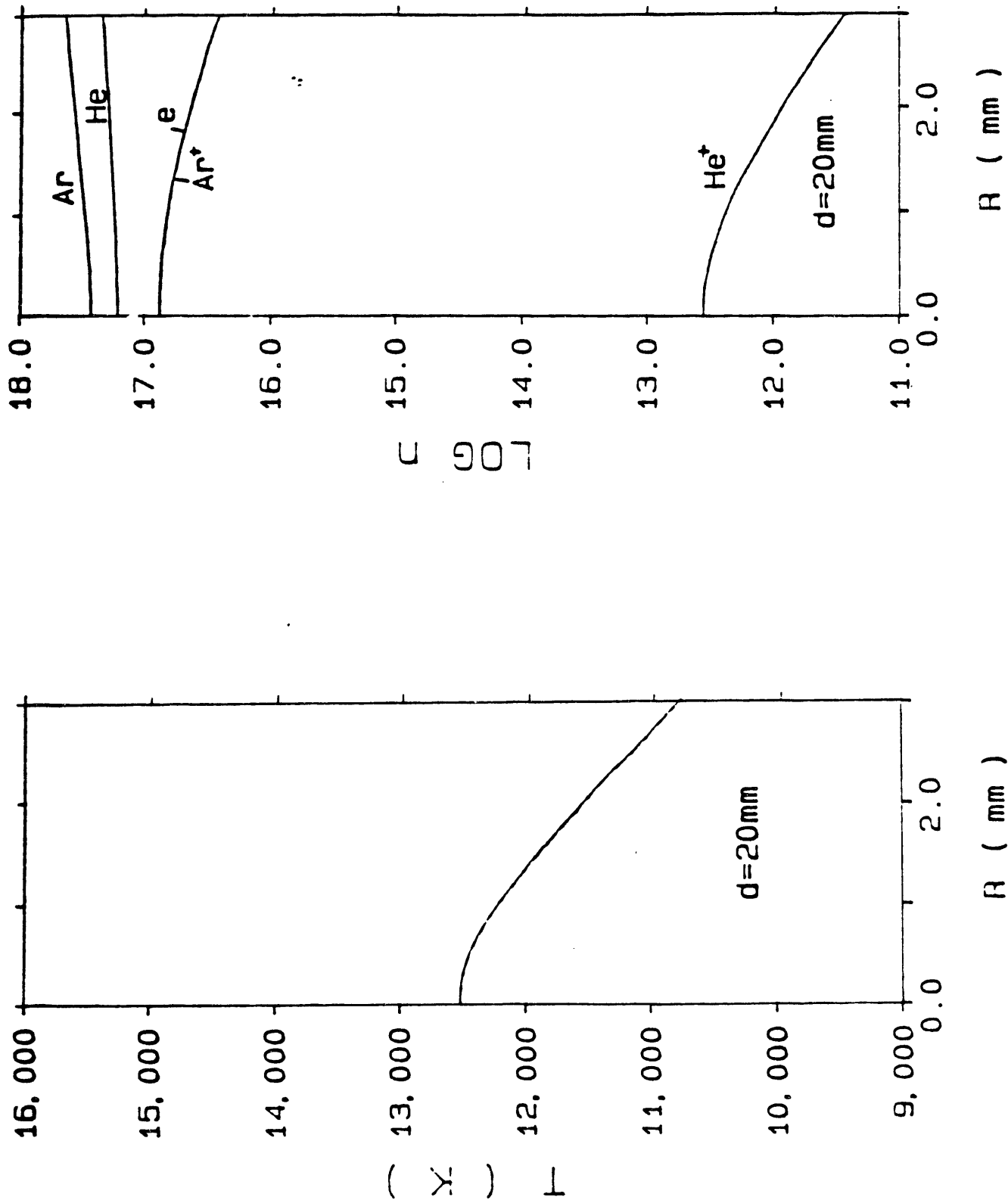


Fig. 26 Temperature and plasma composition profiles assuming LTE and derived from spectroscopic measurements ($d = 20\text{mm}$).

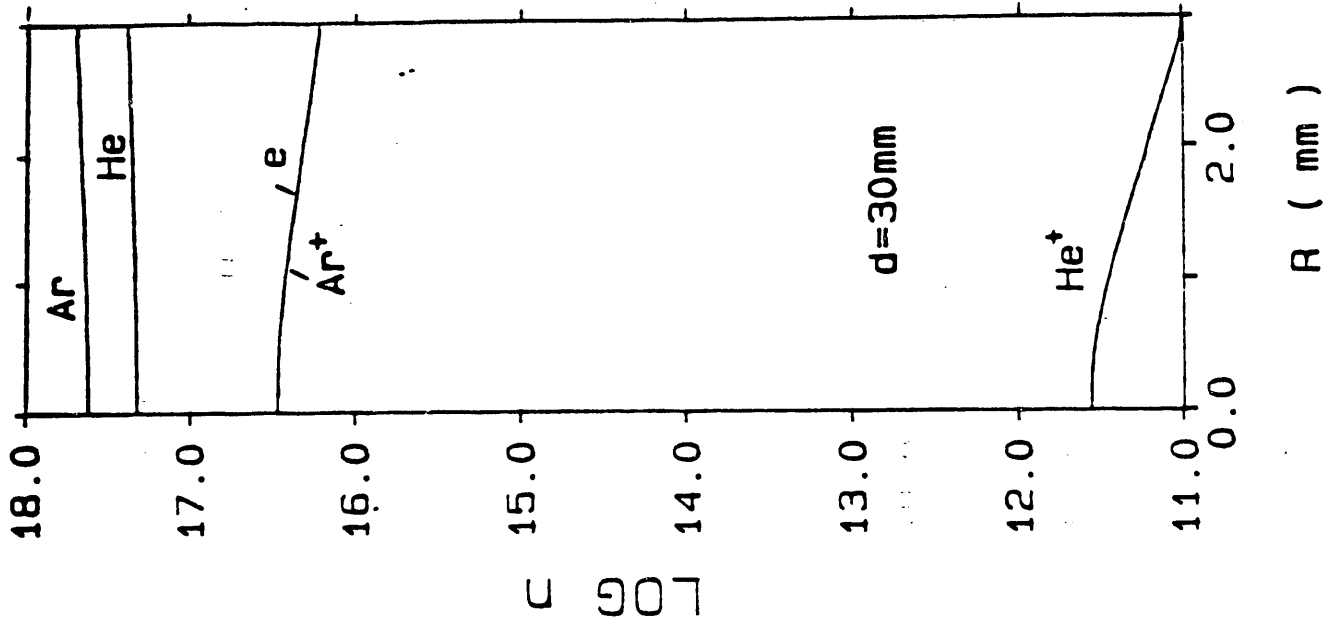
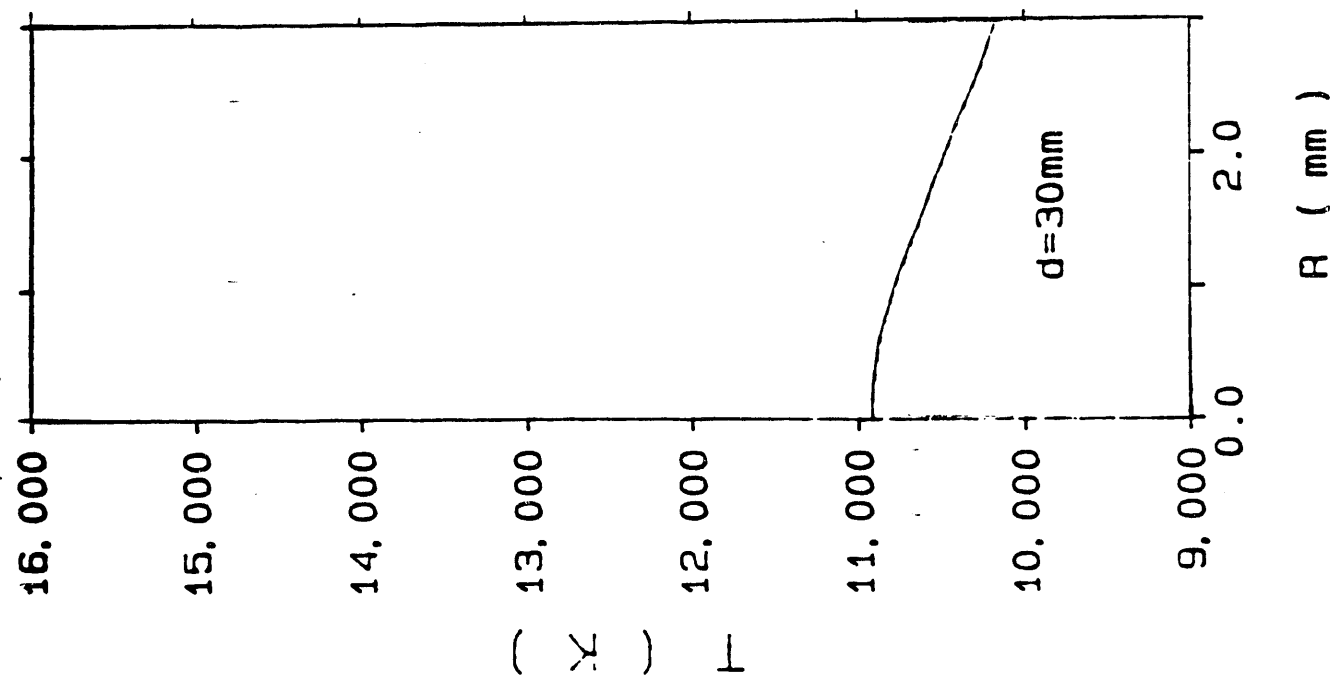


Fig. 27 Temperature and plasma composition profiles assuming LTE and derived from spectroscopic measurements ($d = 30\text{mm}$).

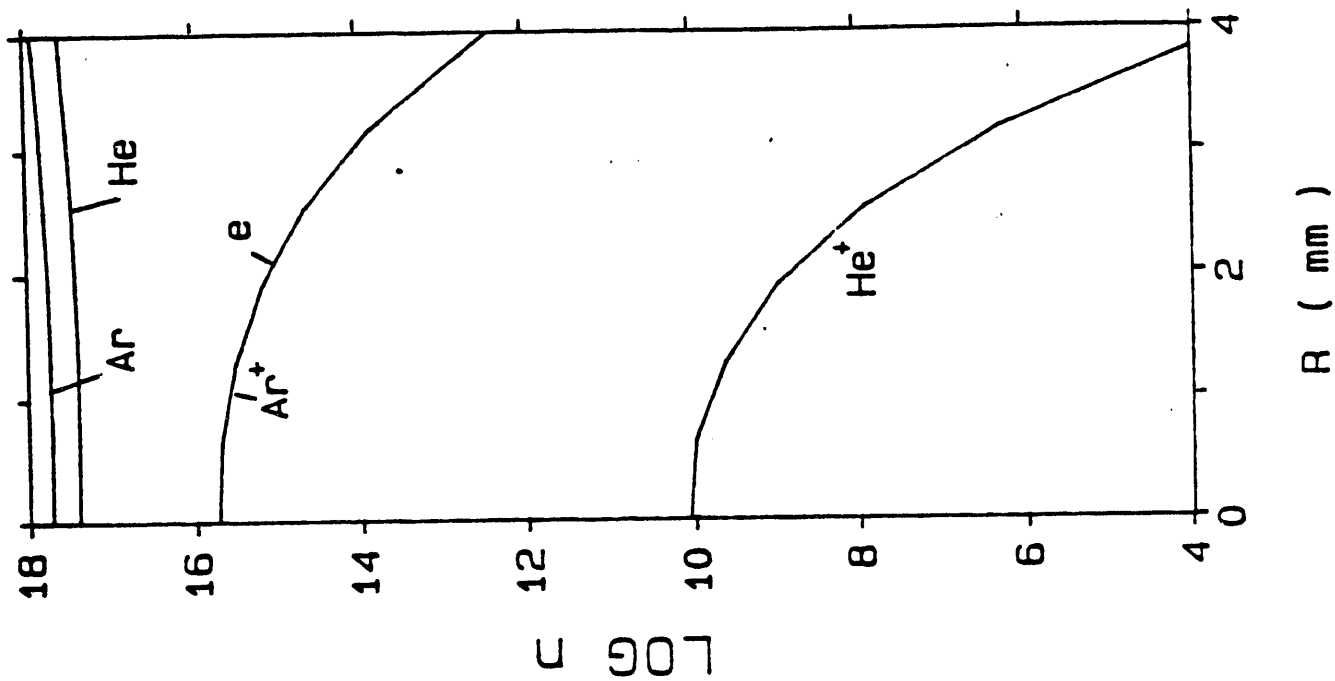
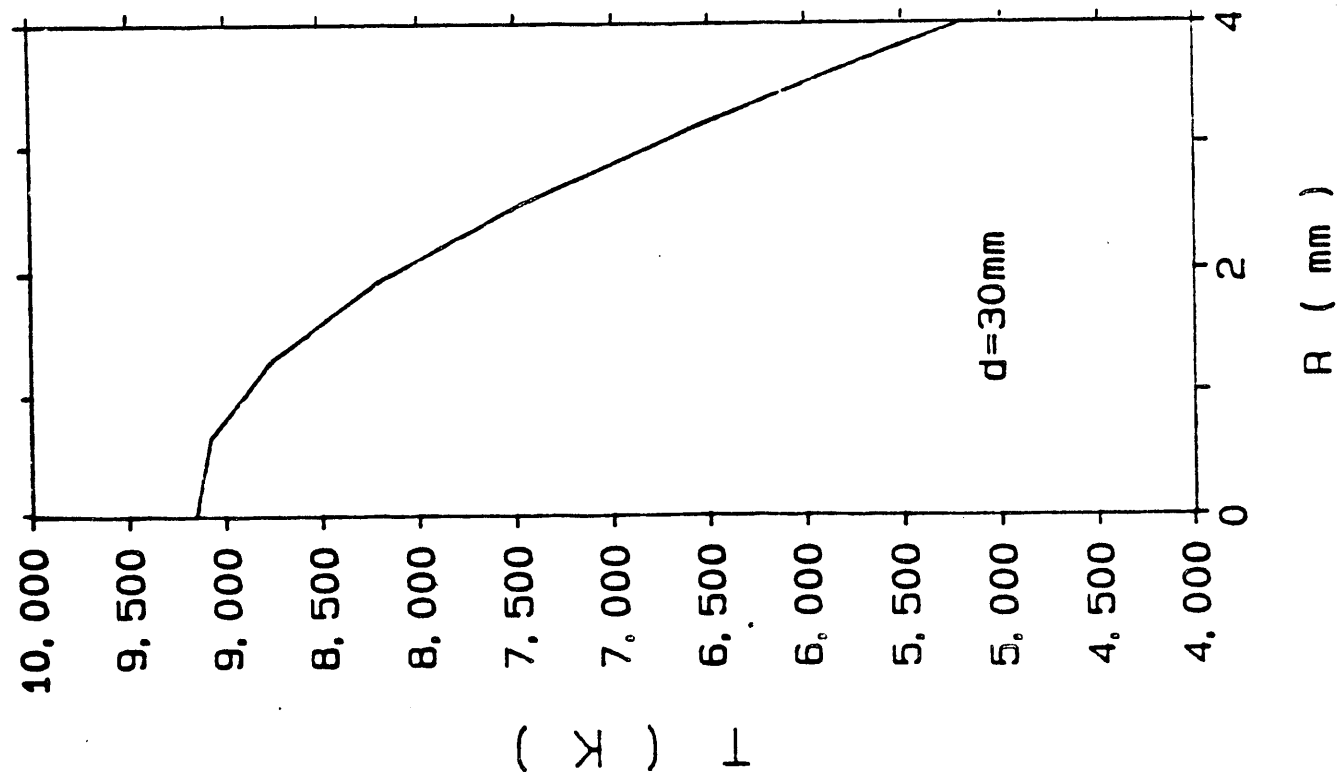


Fig. 28 Temperature and plasma composition profiles assuming LTE and derived from enthalpy probe measurements ($d = 30\text{mm}$).

Table 1. Errors in the energy balance of enthalpy probe measurements

d (mm)	Error in the energy balance (%)
30	- 12.1
35	- 11.6
40	- 20.5
45	- 18.2
50	- 17.9
55	- 10.3

Table 2. Temperature deviations in plasma jets between spectroscopic and enthalpy probe measurements:

ΔT ----- T I R	Gas Flow Ar: 75 (SCFH)					Ar:100 He: 47	Dominant Effect
	300A	400A	500A	600A	800A	800A	
0 mm	<5%	<5%	<5%	<5%	<5%	20%	Diffusion, LTE
2 mm	22%	12%	10%	8%	18%	28%	
3 mm	80%	40%	25%	22%	48%	45%	Cold Gas Entrainment, Non-LTE
d (mm)	15	20	25	30	30	30	
T (R=0,d)	10660	10850	10910	10120	10900	9150 K	

where, $\Delta T = T_{\text{spec}} - T_{\text{probe}}$, $T = T_{\text{probe}}$,

I = arc current ,

R = radius from jet centerline ,

d = distance from nozzle exit.

END

**DATE
FILMED**

12 126 191

